**Forschungszentrum Karlsruhe**
in der Helmholtz-Gemeinschaft

**Wissenschaftliche Berichte**
FZKA 6996

# Stellar Neutron Capture Cross Section of the Unstable Branching Point $^{151}$Sm

**K. Wisshak, F. Voss, F. Käppeler, M. Krtička, S. Raman**

**Institut für Kernphysik**

**Juni 2004**

FORSCHUNGSZENTRUM KARLSRUHE
in der Helmholtz-Gemeinschaft
Wissenschaftliche Berichte
FZKA 6996

# STELLAR NEUTRON CAPTURE CROSS SECTION OF THE UNSTABLE BRANCHING POINT $^{151}$Sm

K. WISSHAK, F. VOSS, F. KÄPPELER, M. KRTIČKA[1], and S. RAMAN[2,†]

Institut für Kernphysik

[1] Charles University Prague, Czech Republic
[2] Oak Ridge National Laboratory, USA
[†]deceased

Forschungszentrum Karlsruhe GmbH, Karlsruhe
2004

**Impressum der Print-Ausgabe:**

**Als Manuskript gedruckt**


**Forschungszentrum Karlsruhe GmbH**
**Postfach 3640, 76021 Karlsruhe**

**Mitglied der Hermann von Helmholtz-Gemeinschaft**
**Deutscher Forschungszentren (HGF)**

**ISSN 0947-8620**

**urn:nbn:de:0005-069969**

# ABSTRACT

The neutron capture cross sections of the radioactive isotope $^{151}$Sm and of natural samarium have been measured in the energy range from 3 to 225 keV at the Karlsruhe 3.7 MV Van de Graaff accelerator. Neutrons were produced via the $^{7}$Li$(p,n)^{7}$Be reaction by bombarding metallic Li targets with a pulsed proton beam and capture events were registered with the Karlsruhe $4\pi$ Barium Fluoride Detector. The cross sections were determined relative to the gold standard using a 206 mg sample of samarium oxide with 90% enrichment in $^{151}$Sm. Over most of the measured energy range uncertainties of $\sim$2-3% could be achieved. The Maxwellian averaged neutron capture cross section of $^{151}$Sm was calculated for thermal energies between $kT = 8$ keV and 100 keV. Together with the result from a parallel measurement at the CERN n_TOF facility on the same sample, this is the first experimental result for the neutron capture cross section of this important branching point isotope in the reaction path of the astrophysical $s$-process. The measured $^{151}$Sm cross section is systematically larger than all theoretical calculations used in previous $s$-process analyses.

# ZUSAMMENFASSUNG

## DER STELLARE (n,$\gamma$)-QUERSCHNITT DES RADIOAKTIVEN VERZWEIGUNGSISOTOPS $^{151}$Sm

Die Neutroneneinfangquerschnitte des radioaktiven Isotops $^{151}$Sm und von natürlichem Samarium wurden am Karlsruher 3.7 MV Van de Graaff Beschleuniger im Energiebereich von 3 bis 225 keV gemessen. Neutronen wurden über die $^{7}$Li$(p,n)^{7}$Be–Reaktion durch Beschuss metallischer Li–Targets mit einem gepulsten Protonenstrahl erzeugt, und Einfangereignisse mit dem Karlsruher $4\pi$ Barium Fluorid Detektor nachgewiesen. Die Messung wurde relativ zum Gold Standard–Querschnitt mit einer Probe aus 206 mg Samariumoxyd durchgeführt, die zu 90% in $^{151}$Sm angereichert war. Insgesamt wurde eine Unsicherheit von $\sim$2-3% erreicht. Aus diesen Daten wurde der stellare Einfangquerschnitt von $^{151}$Sm für thermische Energien von $kT = 8$ keV bis 100 keV berechnet. Zusammen mit dem Ergebnis einer an derselben Probe parallel durchgeführten Messung an der n_TOF Anlage am CERN ist dies der erste experimentelle Wert für dieses wichtige Verzweigungsisotop im Reaktionspfad des astrophysikalischen $s$-Prozesses. Der gemessene $^{151}$Sm Querschnitt ist systematisch größer als alle theoretischen Vorhersagen, die in früheren $s$-Prozess-Analysen verwendet wurden.

# Contents

# 1 INTRODUCTION

The experimental program with the Karlsruhe $4\pi BaF_2$ detector is focused on measurements of keV neutron capture cross sections of relevance for $s$-process nucleosynthesis. The main interest of these studies was concentrated on the main component of the $s$ process, which takes place in thermally pulsing asymptotic giant branch (TP-AGB) stars. This scenario is responsible for about half of the observed abundances between Zr and Bi.

Apart from neutron magic nuclei, the isotopes in this mass range are characterized by comparably large stellar neutron capture cross sections, typically ranging between 100 mb to 1000 mb at a thermal energy of $kT = 30$ keV. Since highly enriched sample material is available in most cases, all relevant stable isotopes of a particular element were studied simultaneously in a standard experiment. Samples typically 0.5 g to 2 g in mass were mounted on a sample ladder and cyclically measured relative to the gold sample as a cross section standard. With this technique corrections for isotopic impurities in the samples could be reliably determined, yielding stellar cross sections with uncertainties around 1%. So far stellar cross sections of 60 isotopes have been measured in the range between $^{93}$Nb and $^{181}$Ta. This data set comprises 16 of the $s$-only isotopes, which are especially important for $s$-process studies since they are shielded from possible $r$-process contributions. Most of these results were already considered in a recent update of evaluated stellar (n,$\gamma$) rates [1].

In the course of this extensive work the experimental method was continuously refined. With a number of improvements more difficult problems could be tackled, e.g. measurements on xenon isotopes [2] where highly enriched gas samples of less than 600 mg in low mass titanium spheres 10 mm in diameter were used. An even more difficult measurement was carried out on nature's rarest stable isotope [3] using a sample containing just 6.7 mg of $^{180m}$Ta with an enrichment of only 5.5%.

The present work on $^{151}$Sm constitutes a further challenge since it is the first measurement on a highly radioactive sample. This isotope is one of the important branching points in the neutron capture chain of $s$-process nucleosynthesis. The strength of this branching is strongly dependent on physical parameters of the stellar site, e.g. on neutron density, temperature, and electron density, thus carrying important information for stellar models. The neutron capture cross section $^{151}$Sm is a crucial part of the nuclear physics input for a thorough branching analysis and is, therefore, required with good accuracy.

The $s$-process reaction path in the vicinity of samarium is sketched in Fig. 1. This region is characterized by the four $s$-only isotopes $^{148,150}$Sm and $^{152,154}$Gd, which are shielded against possible $r$-process contributions by their stable Nd or Sm isobars. Because $^{150}$Sm is not affected by any branching its abundance can, therefore, be used for normalization of the total $s$-process reaction flow. The abundance of $^{152}$Gd is, however, strongly influenced by the branching at $^{151}$Sm. The strength of the right arm of this branching to $^{152}$Sm is

determined by the neutron capture rate

$$\lambda_n = n_n \times \mathrm{v_T} \times \langle\sigma\rangle$$

where $n_n$ stands for the neutron density, $\mathrm{v_T}$ for te mean thermal velocity, and $\langle\sigma\rangle$ for the stellar (n,$\gamma$) cross section. The left arm is proportional to the $\beta^-$ decay rate of $^{151}$Sm, which is significantly enhanced at $s$-process temperatures compared to the terrestrial value of 93 y due to the population of excited nuclear states by the thermal photon bath. The minor branching at $^{152}$Eu has only a marginal effect on the $^{152}$Gd abundance, whereas there might be an additional contribution from the $p$ process.

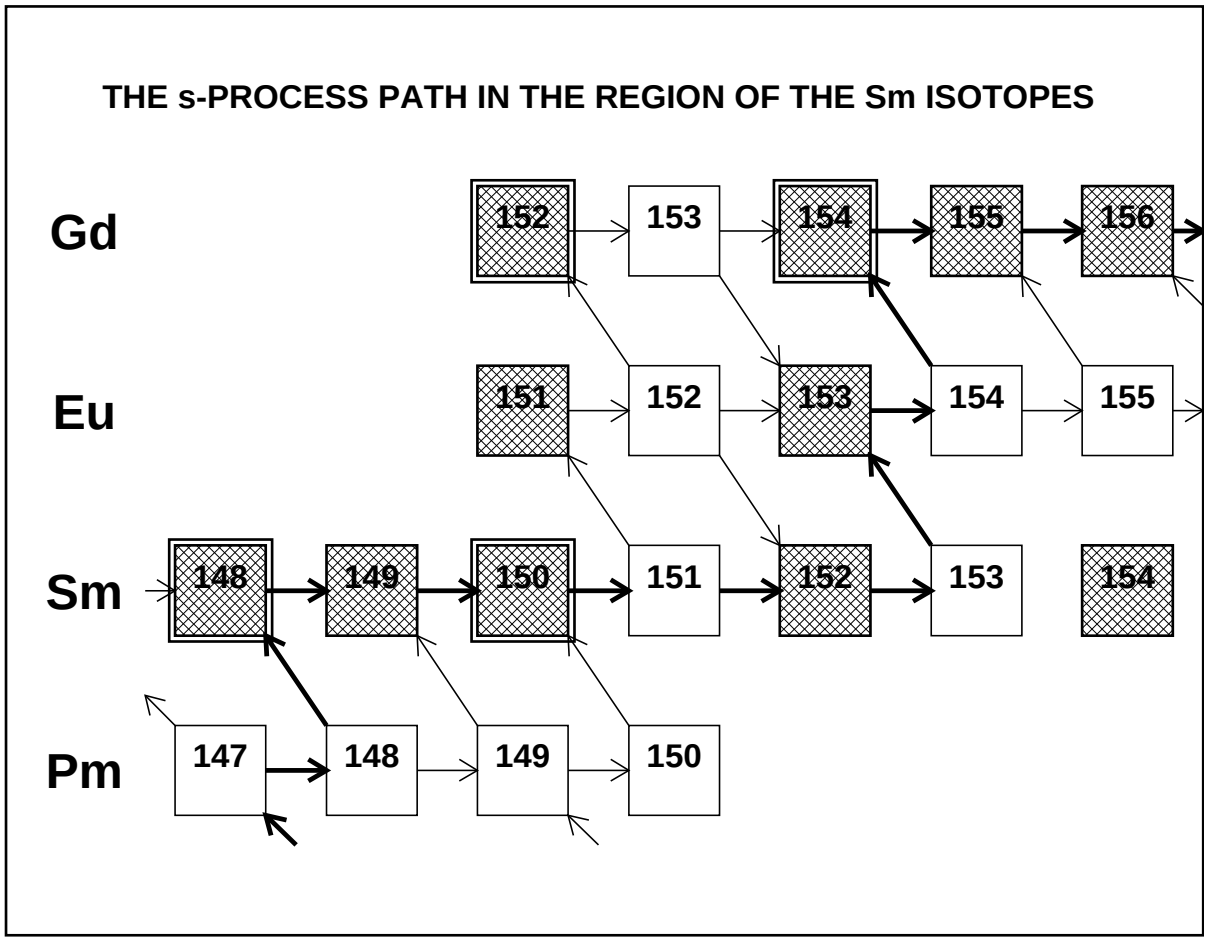


Figure 1: The reaction path of the $s$ process in the region of $^{151}$Sm. Note that $^{148,150}$Sm and $^{152,154}$Gd represent $s$-only isotopes since they are shielded against $\beta$-decays from the $r$-process region by stable Nd or Sm isobars,respectively. Important branchings occur at $^{151}$Sm and $^{152,154}$Eu.

The $^{151}$Sm branching was first analyzed in 1984 based on activation measurements on some Sm, Eu, and Gd isotopes [4]. An improved data set was established in 1986 by a time of flight experiment on three samariumm isotopes including the important $s$-only nuclei [5]. For the stable isotopes involved, the data basis in this mass range was

decisively extended by measurements on five samarium and six Gadolinium isotopes with the Karlsruhe $4\pi$BaF$_2$ detector in 1993-95 [6, 7], which could be used to derive an updated value for the $s$-process neutron density [8]. Recently, the branchings were discussed again [9] in the light of improved cross sections of the stable Eu isotopes.

The only cross section measurements on radioactive branch points in the mass region of interest here were measured for $^{147}$Pm [10] and for $^{155}$Eu [11] by means of the activation technique. Since the activation technique can not be applied for the determination of the $^{151}$Sm cross section, all previous branching analyses had to resort to theoretical values for this important isotope. For a thermal energy of $kT$=30 keV these calculated cross sections varied between 1542 mb and 2809 mb [1], indicating that the respective uncertainties were much too large for meaningful branching analyses.

The obvious need for a measurement of this cross section prompted a collaboration between the research center Karlsruhe and Oak Ridge National Laboratory to prepare an appropriate sample. It was agreed to use this sample in a measurement with the Karlsruhe $4\pi$BaF$_2$ detector in the neutron energy range from 3 keV to 225 keV and in a complementary measurement with an optimized pulse height weighting technique at the newly established n_TOF facility at CERN [12] in the energy range from thermal up to about 1 MeV. Preliminary results of both experiments have been presented in Ref. [13] indicating that the neutron capture cross section of $^{151}$Sm is significantly larger than the calculated values mentioned above.

Measurements and data analysis are described in Secs. 2 and 3, followed by a description of computer simulations with the GEANT code in Sec 4. The discussion of the results and uncertainties is given in Secs. 5 and 6. The stellar cross sections are presented in Sec. 7. The astrophysical implications will be addressed in a forthcoming publication.

# 2 EXPERIMENT

The neutron capture cross section of $^{151}$Sm has been measured in the energy range from 3 to 225 keV using gold as a standard. Since the experimental method has been published in detail [6, 14], only a general description is given here, complemented with the specific features of the present measurement.

Neutrons were produced via the $^7$Li$(p,n)^7$Be reaction by bombarding metallic Li targets with the pulsed proton beam of the Karlsruhe 3.7 MV Van de Graaff accelerator. The neutron energy was determined by time of flight (TOF), the samples being located at a flight path of 79 cm. The relevant parameters of the accelerator were a pulse width of $<$1 ns, a repetition rate of 250 kHz, and an average beam current of 2.0 $\mu$A. In different runs, the proton energy was adjusted 30 and 100 keV above the threshold of the $^7$Li$(p,n)^7$Be reaction at 1.881 MeV. In this way, continuous neutron spectra in the proper energy range for $s$–process studies were obtained, ranging from 3 to 100 keV, and 3 to 225 keV, respectively. The lower maximum neutron energy offers a significantly better signal-to-background ratio at lower energies.

Capture events were registered with the Karlsruhe $4\pi$ Barium Fluoride Detector via the prompt capture $\gamma$–ray cascades. This detector consists of 42 hexagonal and pentagonal crystals forming a spherical shell of BaF$_2$ with 10 cm inner radius and 15 cm thickness. It is characterized by a resolution in $\gamma$–ray energy of 7% at 2.5 MeV, a time resolution of

500 ps, and a peak efficiency of 90% at 1 MeV. The 1.7 MeV threshold in $\gamma$–ray energy used in the present experiment corresponds to an efficiency for capture events of more than 95%. A comprehensive description of this detector can be found in Ref. [15].

The experiment was divided into three runs, two using the conventional data acquisition technique with the detector operated as a calorimeter, and one with an analog-to-digital converter (ADC) system coupled to the detector for analyzing the signals from all modules individually. In this way, the full spectroscopic information recorded by the detector can be recovered.

The aquisition of a suited $^{151}$Sm sample started already in 1990 while preparing the experiment on the stable Sm isotopes [6]. Attempts to get hold of the metallic sample used in 1975 by Kirouac and Eiland for a measurement of the total cross section [16] were eventually successful in 1998 when ORNL agreed to reprocess the old sample for separating the decay product $^{151}$Eu by liquid chromatography in an ion-exchange column. By sharing the costs of 25000 US$ for this procedure between ORNL and FZK a suited sample could be made from the purified sample material, which was converted into samarium oxide.

Before pressing into a solid pellet, the samarium oxide was heated to high temperatures to ensure the proper stoichiometry and to eliminate possible water contaminations. The pellet was then enclosed in a Ti can, which was prepared from 0.25 mm thick titanium metal sheets and consisted of a deep-drawn body 15 mm in diameter with a 3 mm depression 10 mm in diameter for the sample pellet. The lid had a corresponding 1 mm depression to match the 2 mm thick pellet. The can was sealed by electron beam welding at the outer circumference of body and lid.

An identical sample, which was first prepared from natural samarium oxide to verify the procedure, was also used in the experiment to check whether the correct values for the much smaller cross section of natural samarium could be reproduced.

Apart from the two samarium samples, a gold sample in an identical can was used for measuring the neutron flux, and an empty can served for determining the sample-independent background. The background due to scattered neutrons was measured by means of a graphite sample. The relevant sample parameters are compiled in Table 1.

For the radioactive sample the changes in isotopic composition with time were followed in detail. The isotopic composition was determined at ORNL immediately after the Eu separation. When the sample was shipped to FZK 1.5 years later a corrected isotopic composition was declared by ORNL with a difference in $^{151}$Sm corresponding to the ingrowth of $^{151}$Eu. The measurements at FZKA were started in December 2001, but most of the data taking took place between October 2002 and January 2003. The composition at the end of November 2002 was taken into account in the analysis of these measurements as given in Table 2. While the isotopic composition of samarium was almost constant since the separation, the mass had changed by about two percent due to the ingrowth of $^{151}$Eu. This impurity required a significant correction since $^{151}$Eu has the largest capture cross section of all stable isotopes in this mass range.

In the work of Kirouac and Eiland [16] the reference date for the quoted isotopic composition is not given. Assuming that it was determined at the time of their experiment in 1974 would result in a relative $^{151}$Sm abundance of 91.81%, higher than measured during the chemical separation in 1999 (Table 2). This difference suggests that the isotopic composition quoted in Ref. [16] had been determined already 25 years earlier. This

Table 1: SAMPLE CHARACTERISTICS

| Sample | Diameter | Thickness | | Weight | Can[b] | Neutron binding |
|---|---|---|---|---|---|---|
| | (mm) | (mm) | ($10^{-3}$at/barn)[a] | (g) | (g) | energy (MeV) |
| Graphite | 10.0 | 1.0 | 8.7427 | 0.1370 | 0.4349 | |
| $^{197}$Au | 10.0 | 0.4 | 2.1621 | 0.5554 | 0.4329 | 6.513 |
| $^{151}$Sm[c] | 10.0 | 0.6 | 0.8861 | 0.2064 | 0.4340 | 8.258 |
| $^{nat}$Sm[c] | 10.0 | 0.6 | 0.9675 | 0.2200 | 0.3989 | 5.6-8.1 |
| Empty | | | | | 0.4181 | |

[a]For Sm samples: sum of all Sm isotopes
[b]Welded titanium can 15 mm in diameter, lid and body deep-drawn from 0.25 mm thick foils.
[c]Chemical form $Sm_2O_3$

assumption is confirmed by the balance of the absolute $^{151}$Sm mass. The 256.1mg of samarium metal with 93.11 enrichment reported in Ref. [16] corresponds to a $^{151}$Sm mass of 238.4 mg. The decay over a period of 50 years leaves a 164.3 mg, in good agreement with the 160.4 mg $^{151}$Sm remaining in the sample after the separation in 1999 if the oxygen content is properly considered.

Table 2: ISOTOPIC COMPOSITION (%)

| Isotope | Date (m-d-y) | | |
|---|---|---|---|
| | Eu separation | shipping | measurement |
| | 10-28-1999 | 5-21-2001 | 11-28-2002 |
| | Composition (%) | | |
| $^{144}$Sm | 0.05 | 0.051 | 0.052 |
| $^{147}$Sm | 1.37 | 1.384 | 1.398 |
| $^{148}$Sm | 0.22 | 0.222 | 0.224 |
| $^{149}$Sm | 0.40 | 0.404 | 0.408 |
| $^{150}$Sm | 3.93 | 3.972 | 4.013 |
| $^{151}$Sm | 90.05 | 89.945 | 89.842 |
| $^{152}$Sm | 3.32 | 3.355 | 3.389 |
| $^{154}$Sm | 0.66 | 0.667 | 0.674 |
| mass $Sm_2O_3$ (mg) | 206.4 | 204.24 | 202.16 |
| mass $Eu_2O_3$ (mg) | 0.0 | 2.16 | 4.24 |

The neutron transmission of the samples calculated with the SESH code [17] was generally larger than 95% (Table 3). The measured spectra of all samples were normalized to equal neutron flux by means of a $^6$Li–glass monitor located close to the neutron target. The transmission spectra measured with a second $^6$Li–glass detector with 30 mm diameter at a flight path of 260 cm could again be used for a rough determination of the total cross

sections, since the sample diameter of 10 mm is just sufficient to shade the neutron monitor completely.

The samples were moved cyclically into the measuring position by a computer controlled sample changer. In contrast to our previous experiments the distance of the samples in the ladder was reduced from ∼6 to 4 cm. This has the advantage that the $^{151}$Sm sample which was mounted in the central position (see Table 1) was always completely within the inner radius of the spherical $BaF_2$ shell. In this way the background induced by the radioactivity of the sample was similar for all samples.

Table 3: CALCULATED NEUTRON TRANSMISSION[a]

| Sample | Neutron Energy (keV) | | | | |
|---|---|---|---|---|---|
| | 10 | 20 | 40 | 80 | 160 |
| $^{197}$Au | 0.961 | 0.966 | 0.971 | 0.975 | 0.979 |
| $^{151}$Sm | 0.973 | 0.978 | 0.982 | 0.985 | 0.988 |
| $^{nat}$Sm | 0.972 | 0.977 | 0.981 | 0.984 | 0.986 |

[a] Monte Carlo calculation with SESH code [17].

The data acquisition time per sample was about 10 min, a complete cycle lasting ∼0.8 h. From each event, a 64 bit word was recorded on DLT tape containing the sum energy and TOF information together with 42 bits identifying the contributing detector modules. The respective parameters of the three runs corresponding to neutron spectra with different maximum energies are listed in Table 4. The data in run III were recorded with the ADC system. Due to unfortunate circumstances data taking of run I was interrupted for nearly a year while it was completed for the two other runs in 2 and 3 weeks, respectively. This was due to extensive repairs of the accelerator and to the fact that the $^{151}$Sm sample was used for two months in a parallel experiment at the CERN n_TOF facility. This delay was compensated by a new record in pulsed proton beam current. During run III a maximum of 2.8 $\mu$A and a total average of 2.4 $\mu$A were reached, the largest values ever achieved at the Karlsruhe Van de Graaff (Table 4).

Table 4: PARAMETERS OF THE INDIVIDUAL RUNS

| Run | Flight Path (mm) | TOF Scale (ns/ch) | Number of Cycles | Maximum Neutron Energy (keV) | Measuring Time (d) | Mode of Operation | Average Beam Current ($\mu$A) | Threshold in Sum Energy (MeV) |
|---|---|---|---|---|---|---|---|---|
| I | 786.9 | 0.746 | 690 | 100 | 23.2 | Calorimeter | 2.1 | 1.7 |
| II | 786.9 | 0.749 | 334 | 200 | 10.8 | Calorimeter | 2.2 | 1.8 |
| III | 786.9 | 0.696 | 402 | 100 | 11.7 | ADC | 2.4 | 1.8 |

# 3 DATA ANALYSIS

## 3.1 Total Cross Sections

The total cross sections of the investigated isotopes were determined in the neutron energy range from 10 to 200 keV via the TOF spectra measured with the $^{6}$Li glass detector at a flight path of 260 cm. The total cross sections and the related uncertainties were obtained as described in Ref. [6], and are listed in Table 5. For easier comparison of the individual results the averaged total cross sections in the neutron energy interval from 10 to 100 keV are included in the table. The results deduced for the carbon sample agree within $\pm 1.2\%$ with the data from the Joint Evaluated File (JEF) [18] given in the $7^{th}$ column of the table. Since our first determination of the total cross sections of carbon and gold during the experiment on the stable samarium isotopes [6] published in 1993 the same cross sections were redetermined in nine further experiments on isotopes of other elements (Ba, Gd, Sn, Nd, Dy, Yb, Cd, Lu, and Hf). A survey of this large amount of data showed that rather consistent results were obtained using samples of different diameter (15, 22 mm) and thicknesses (1.4 - 4.9 mm). The averaged values of these ten experiments are given in Table 5 in the columns labeled previous. The present results which were obtained with samples of 10 mm in diameter agree with these data. The cross section of natural samarium was calculated from the values given in Ref. [6] with the assumption that the total cross section of $^{144,154}$Sm, which were not included in the experiment, are the same as measured for the neighboring even isotopes $^{148,152}$Sm. This crude evaluation is in fairly good agreement with the present experiment (see Table 5). Both data sets are found in reasonable agreement with the data given in Ref. [19].

Table 5: MEASURED TOTAL CROSS SECTIONS [a]

| Neutron Energy | Total Cross Section (barn) | | | | | | | |
|---|---|---|---|---|---|---|---|---|
| | $^{151}$Sm | $^{nat}$Sm | | $^{12}$C | | | $^{197}$Au | |
| (keV) | present | present | Ref.[6] | present | previous | JEF | present | previous |
| 10 – 15 | 26.7 | 19.8 | 21.1 | 4.74 | 4.57 | 4.69 | 19.0 | 15.7 |
| 15 – 20 | 37.9 | 22.7 | 17.4 | 4.58 | 4.54 | 4.67 | 18.5 | 14.8 |
| 20 – 30 | 25.2 | 17.9 | 17.6 | 4.78 | 4.59 | 4.65 | 15.1 | 14.0 |
| 30 – 40 | 16.9 | 13.6 | 15.2 | 4.31 | 4.39 | 4.61 | 12.7 | 13.2 |
| 40 – 60 | 15.8 | 13.3 | 14.1 | 4.61 | 4.54 | 4.56 | 12.3 | 12.3 |
| 60 – 80 | 11.7 | 10.6 | 12.4 | 4.33 | 4.44 | 4.49 | 10.5 | 11.4 |
| 80 – 100 | 12.5 | 12.1 | 11.6 | 4.37 | 4.22 | 4.42 | 11.4 | 10.8 |
| 100 – 150 | 11.4 | 11.6 | 10.9 | 4.14 | 4.18 | 4.31 | 10.4 | 10.6 |
| 150 – 200 | 10.2 | 11.1 | 9.7 | 3.95 | 3.95 | 4.16 | 9.1 | 9.0 |
| 10 – 100 | 17.16 | 13.86 | 14.25 | 4.49 | 4.44 | 4.54 | 12.77 | 12.38 |
| Typical Uncertainty (%) | 2.1 | 2.2 | 5.3 | 1.2 | 1.1 | | 1.5 | 3.3 |

[a]Determined from the count rate of the $^{6}$Li glass neutron monitor at 260 cm flight path

The quoted uncertainties of the present measurements were obtained under the assumption that they are inversely proportional to the fraction of neutrons interacting in the sample, $A = 1 - T$, where $T$ is the transmission. For the carbon sample this fraction is $A = 4.0\%$, the related uncertainty of 1.2% being estimated from the comparison with the JEF data.

## 3.2 Capture Cross Sections

The analysis was carried out in the same way as described previously [6, 14]. All events were sorted into two–dimensional spectra containing 128 sum energy versus 2048 TOF channels according to different multiplicities (evaluation 1). In evaluation 2, this procedure was repeated by rejecting those events, where only neighboring detector modules contributed to the sum energy signal. With this option, background from the natural radioactivity of the $BaF_2$ crystals and from scattered neutrons can be reduced. For all samples, the resulting spectra were normalized to equal neutron flux using the count rate of the $^6$Li glass monitor close to the neutron target. The corresponding normalization factors are below 0.5% for all runs. The treatment of the two-dimensional spectra from the data recorded with the ADC system is slightly more complicated and was performed as described in Ref. [6].

In the next step of data analysis, sample-independent backgrounds were removed by subtracting the spectra measured with the empty can. A remaining constant background was determined at very long flight times, where no time-correlated events are expected. The resulting two-dimensional spectra for events with multiplicity >2 measured in run III are shown for the $^{151}$Sm and $^{197}$Au samples in Fig. 2. Note that events with low sum energy and large TOF are suppressed by a preprocessing option of the ADC system.

At this point, the spectra contain only events correlated with the sample. The next correction to be made is for isotopic impurities. In the present experiment the samples of the impurity isotopes were not included in the measurement and thus a simple subtraction of the normalized spectra of the impurity isotopes is excluded. From the isotopic contribution in Table 2 and adopting the stellar cross sections at $kT$=30 keV from Ref. [1] one can estimate that 95.2% of the events around 30 keV should be due to capture in $^{151}$Sm. Another 1.8% of events are contributed by capture in the impurity isotopes of samarium and 3.0% by capture in $^{151}$Eu. The 1.8% correction for the Sm isotopes contain contributions of 1.0% and 0.8% from the even and odd isotopes, respectively.

The good resolution in $\gamma$-ray energy of the present setup provides a reliable way for evaluating the correction for isotopic impurities in the investigated region of unresolved neutron resonances. The upper part of Fig. 3 shows the sum-energy spectrum for capture events with multiplicities m>2 measured in the neutron energy interval from 50 keV to 100 keV in run III. The binding energies of $^{151}$Sm and of the various impurity isotopes are indicated by arrows. The relative contributions from the stable Sm isotopes in the lower panel were determined by normalizing the respective spectra (Fig. 5 of Ref. [6]) to the composition of the $^{151}$Sm sample. The purpose of this constructed spectrum is to demonstrate that the impurity contributions are dominated by the full energy peak of the even isotopes at ~5.8 MeV and that the contributions of the odd isotopes are significantly smaller, in agreement with the above estimate.

The comparison with the measured sum-energy spectrum in the upper panel confirms that the part of the structure around 6 MeV corresponds to the sum energy of the even Sm isotopes but that additional events are visible at the binding energy of $^{151}$Eu. It is also obvious that the contribution from the odd Sm isotopes can not be distinguished from the capture events in $^{151}$Sm.

In Fig. 4 the sum-energy spectrum of capture events in $^{151}$Sm is compared to the respective spectra of the two odd isotopes, $^{147}$Sm and $^{149}$Sm (from Fig. 5 of Ref. [6]) as well as with a simulation using the GEANT package (to be described in Sec. 4). From this comparison it could be plausible assumed that the spectrum of capture events in $^{151}$Sm is well represented by a straight line in the energy interval between 2 MeV and 7 MeV . The correction for isotopic impurities was, therefore, performed not by subtraction of the normalized spectra of the impurity isotopes but in the following way.

The energy dependence of the $^{151}$Sm cross section was evaluated by using only events with sum energies above $\sim$6.5 MeV. This excluded automatically the contributions of the even samarium isotopes and of $^{151}$Eu. For the absolute normalization of the cross section, where the sum-energy spectrum had to be integrated in the normalization interval from the adopted threshold at 1.8 MeV to energies above the binding energy (see below) a linear dependence of the spectral shape was assumed, eliminating events above the line shown in Figs. 3, 4.

The remaining background due to capture of sample scattered neutrons was corrected by means of the data measured with the scattering sample. The binding energy of $^{151}$Sm of 8.26 MeV is low enough, that this correction could be normalized via the pronounced sum-energy peak at 9.1 MeV from neutron capture in $^{133}$Ba and $^{135}$Ba (see Fig. 2). The backgrounds for capture of scattered neutrons are indicated in Fig. 5, and the corresponding signal/background ratios are listed in Table 6 for different neutron energies. At this point, the corrected spectra contain only the net capture events of the investigated isotopes (bottom spectra in Fig. 2).

After subtraction of the scattering background the cross section shape versus neutron energy was determined from the TOF spectra of Fig. 5. These spectra are calculated by integrating the two-dimensional spectra in a region around the full energy peak. Due to the different background conditions in the spectra of events with different multiplicities, this range was chosen to decrease with multiplicity (see Fig. 7). As mentioned before this range was restricted for the $^{151}$Sm sample to events above 6.5 MeV. For absolute normalization, the two–dimensional data were projected onto the sum-energy axis using the TOF region with optimum signal/background ratio between the vertical lines indicated in Fig. 5. The resulting pulse height spectra are plotted in Fig. 6 for events with multiplicities $>$2. The spectrum of the natural Sm sample is dominated by the even isotopes. The contribution of the odd isotopes is slightly larger than in the $^{151}$Sm sample (Fig 3) due to the different isotopic composition.

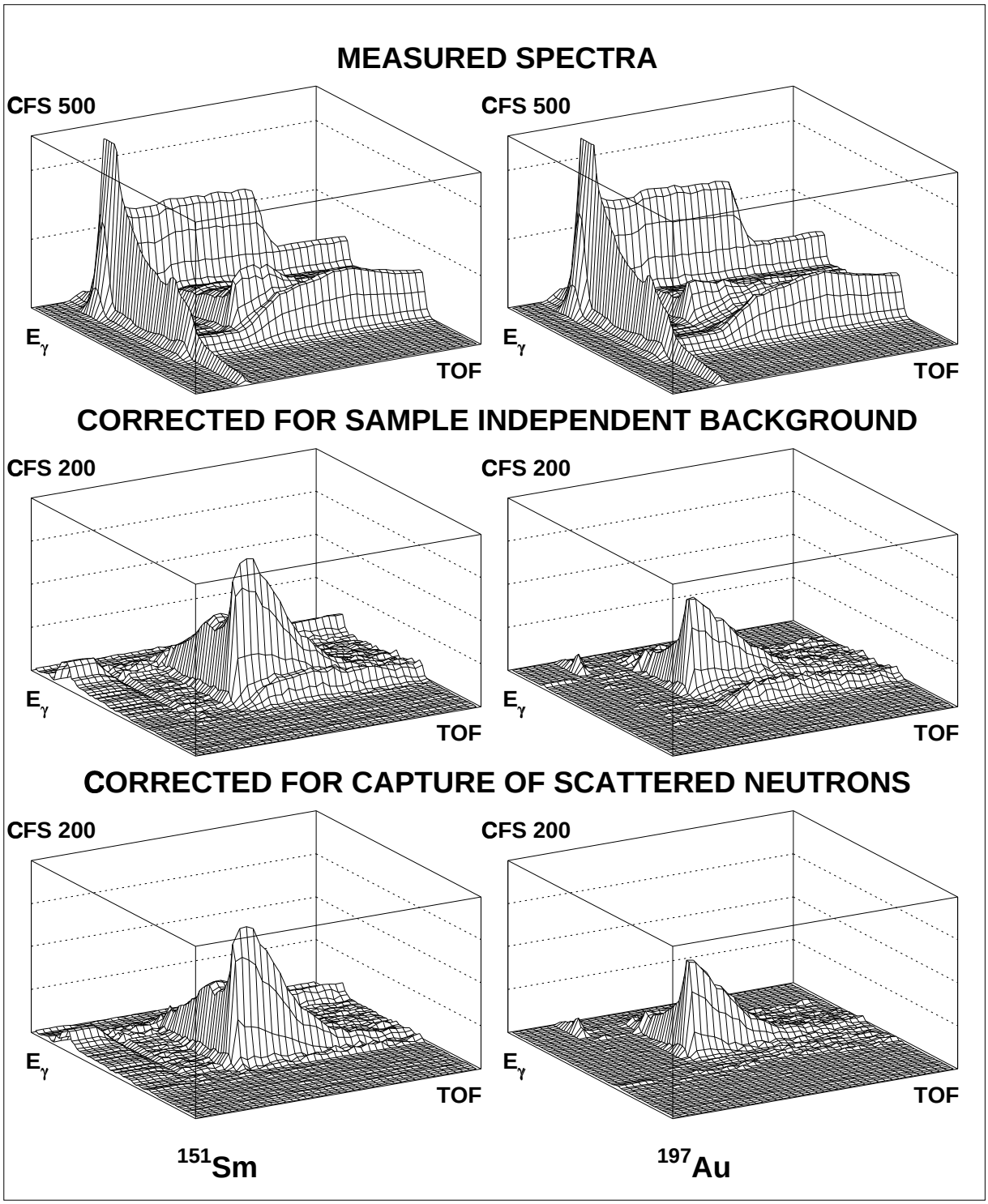


Figure 2: The different steps of background subtraction in the two–dimensional sum energy × TOF spectra illustrated by the data for $^{151}$Sm and $^{197}$Au. These spectra were measured with the ADC system in run III with 100 keV maximum neutron energy and contain events with multiplicities >2 only. (The original resolution of 128 × 2048 channels was compressed into 64 × 64 channels for better readability. Events at low sum-energies and large TOF are suppressed by the preprocessing option of the ADC system.)

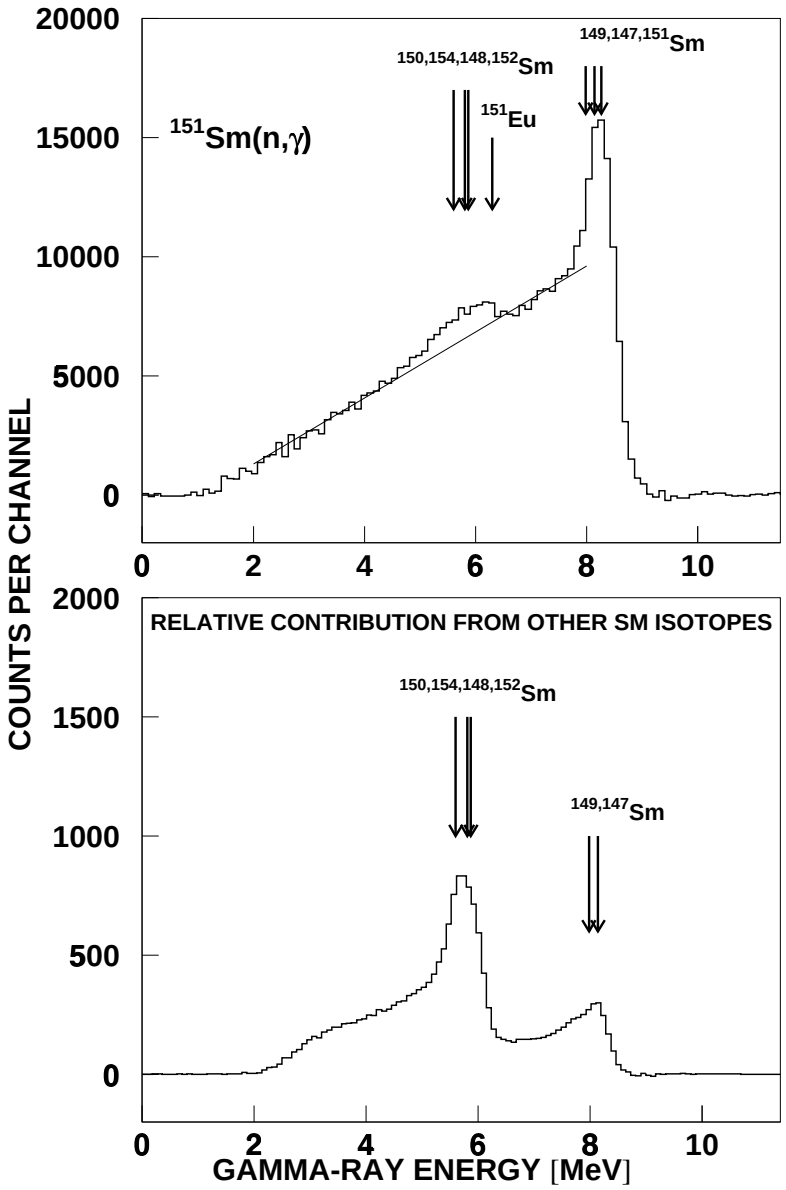


Figure 3: Sum-energy spectrum of capture events measured with the $^{151}$Sm sample in run III showing events with multiplicities >2 (top). The arrows indicate the position of sum-energy peaks of impurity isotopes. The contributions of the other Sm isotopes presented in the bottom panel were obtained by means of the spectra measured in Ref. [6].

The sum energy spectra of all isotopes are shown in Fig. 7 for different multiplicities $m$. These multiplicities correspond to the number of detector modules contributing per event, which are slightly larger than the true multiplicities $m$ because of cross talking. The arrows in Fig. 7 indicate the range of sum energy channels that were integrated to obtain the TOF spectra of Fig. 5 for determining the cross section shapes.

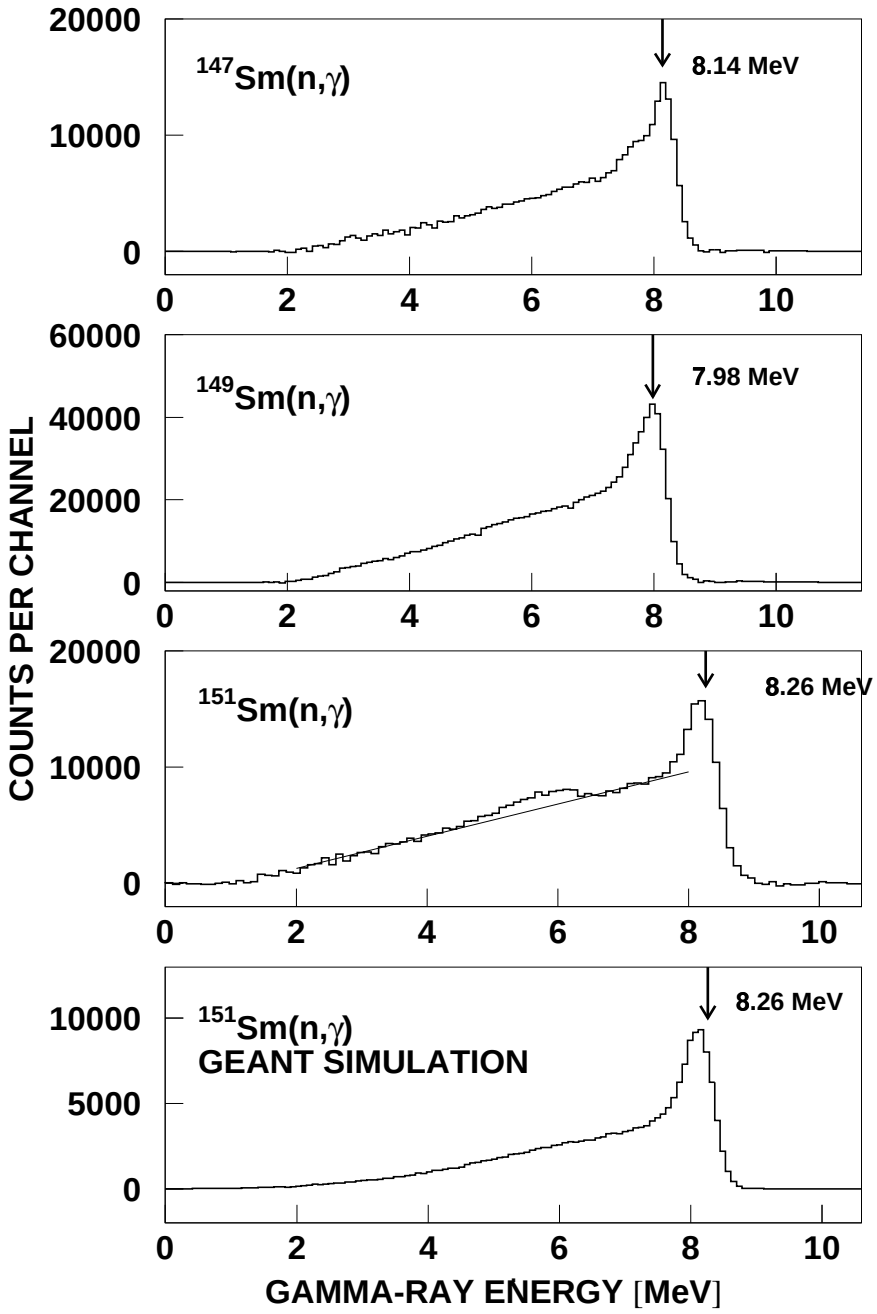


Figure 4: The comparison of the sum-energy spectrum of $^{151}$Sm with the stable odd Sm isotopes [6] and with a GEANT simulation confirms the linear behavior in the energy range between 2 MeV and 7 MeV assumed for evaluating the isotopic correction. All spectra contain only events with multiplicities >2.

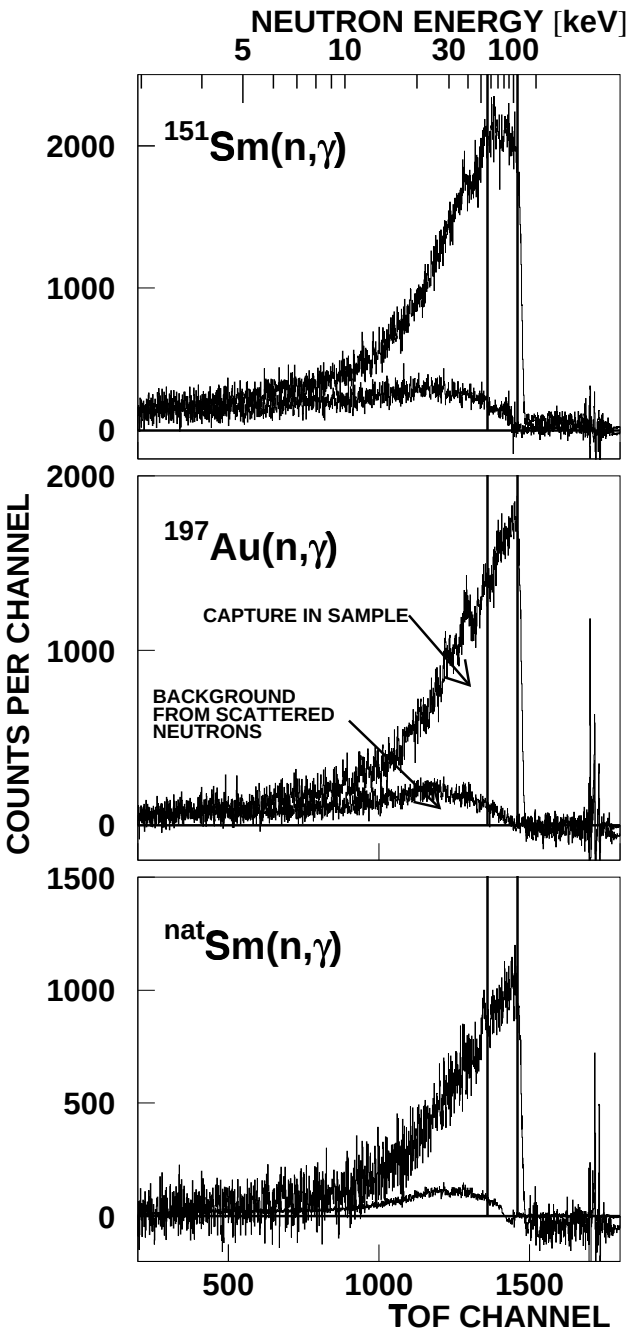


Figure 5: TOF spectra measured in run III (100 keV maximum neutron energy) with the background due to sample scattered neutrons. The region used for absolute normalization of the cross section is indicated by two vertical lines.

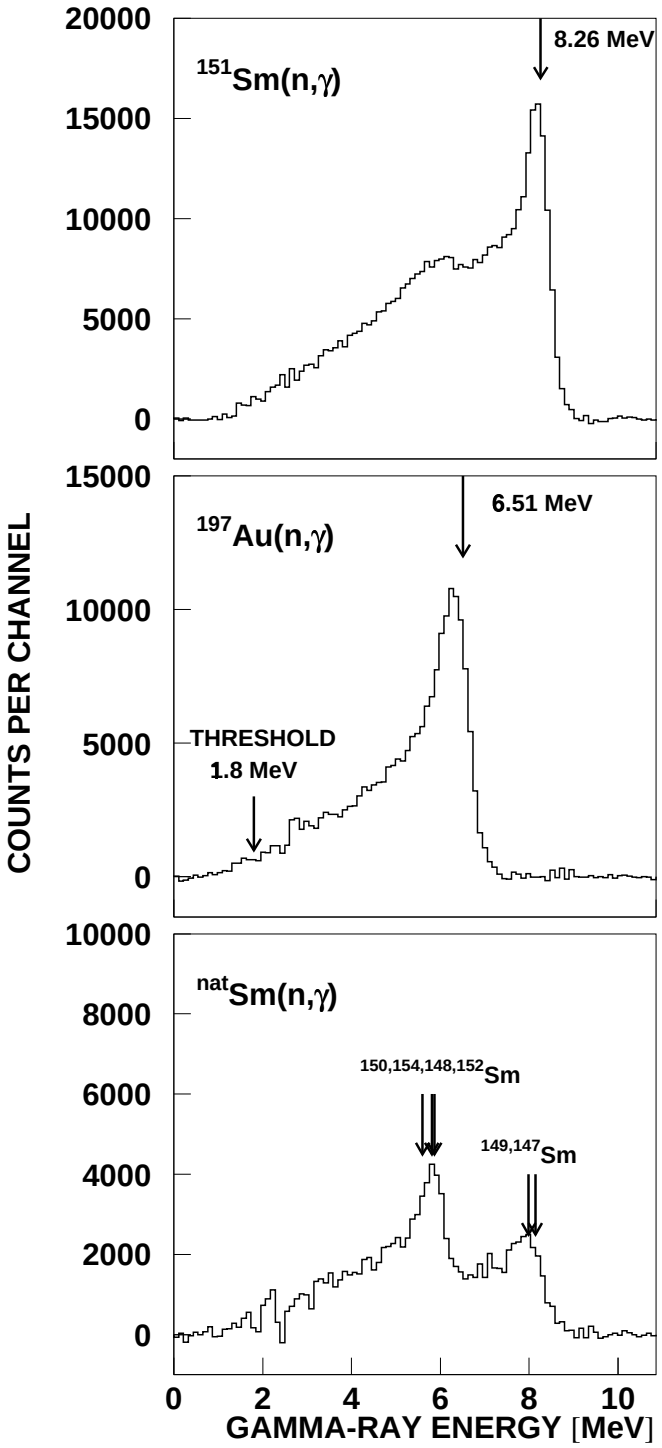


Figure 6: Sum energy spectra measured in run III containing events with multiplicities >2 only. These spectra were obtained by projection of the two–dimensional spectra in the TOF region below the maximum neutron energy as indicated by vertical lines in Fig. 5.

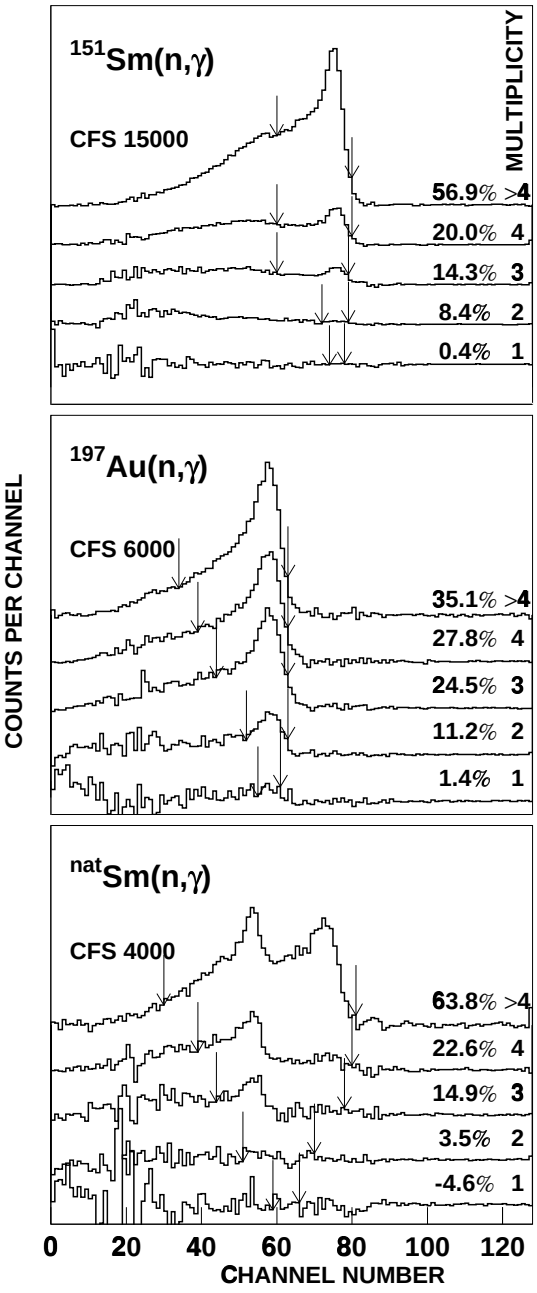


Figure 7: Sum energy spectra of all isotopes as a function of multiplicity (run III). The regions used for determining the cross section shape (see TOF spectra of Fig. 5) are indicated by arrows. In the spectrum of the $^{151}$Sm sample events below 6.5 MeV are excluded to avoid backgrounds from the main isotopic impurities (see text).

Table 6: SIGNAL/BACKGROUND RATIO FOR RUNS WITH DIFFERENT MAXIMUM NEUTRON ENERGY

| Sample | $\sigma_t/\sigma_\gamma$ | Maximum neutron energy | Signal/Background ratio[a] | | |
|---|---|---|---|---|---|
| | $E_n$=30 keV | (keV) | $E_n$=30 keV | $E_n$=20 keV | $E_n$=10 keV |
| $^{151}$Sm | 5 | 100 | 5.5 | 3.3 | 2.0 |
| $^{nat}$Sm | 27 | | 6.0 | 4.5 | 2.5 |
| $^{197}$Au | 24 | | 5.6 | 3.0 | 2.7 |
| $^{151}$Sm | | 200 | 2.9 | 2.2 | 1.6 |
| $^{nat}$Sm | | | 5.5 | 4.0 | 2.4 |
| $^{197}$Au | | | 4.9 | 3.6 | 2.3 |

[a]Defined as (effect+neutron scattering background)/(neutron scattering background)

The cross section ratio of isotope $X$ relative to the gold standard is given by

$$\frac{\sigma_i(X)}{\sigma_i(Au)} = \frac{Z_i(X)}{Z_i(Au)} \frac{\Sigma Z(Au)}{\Sigma Z(X)} \frac{\Sigma E(X)}{\Sigma E(Au)} \frac{m(Au)}{m(X)} F_1 F_2. \quad (1)$$

In this expression, $Z_i$ is the count rate of channel $i$ in the TOF spectrum and $\Sigma Z$ is the TOF rate integrated over the interval used for normalization (vertical lines in Fig. 5). The total count rate in the sum-energy spectra for all multiplicities in this TOF interval, $\Sigma E$, is obtained by integration of the corrected spectra from the 1.8 MeV threshold up to and including the full energy peak at the respective separation energy.

The small number of events at low $\gamma$-ray energies and for multiplicities 1 and/or 2 contribute most of the statistical uncertainty. These contributions to $\Sigma E$ were usually determined by extrapolation as described in Ref. [20]. This method did not apply in the present case since the required statistical accuracy could not be obtained in all runs due to the small samples used. Therefore, the full statistical uncertainty of events with multiplicity 1 had to be taken into account, which is similar to the combined statistical uncertainty of all spectra with multiplicities $> 1$.

From the previous Sm measurements [6] it was known that the spectrum with multiplicitiy 1 contribute only a very small fraction to $\Sigma E$ for the odd isotopes. This was also confirmed for $^{151}$Sm, where the GEANT simulations yielded a contribution of 0.6%, in good agreement with the data of run III (Fig. 7). Similarly good agreement compared to Ref. [6] was found for the multiplicity distribution of the gold sample as well. The situation in the two other runs was less consistent though. In run I data were collected with a long interruption of almost a year while run II fell in a period of unstable accelerator conditions. In both cases the contributions from the spectra with multiplicities $\leq 2$ appeared to be rather unphysical and were corrected to comply with the values obtained in run III. For example, in run II the contribution for multiplicity 1 in the $^{151}$Sm sample was 11% and even negative values were found for the gold sample as well as for multiplicity 2 of the $^{151}$Sm sample. In run I the contribution of $^{151}$Sm events with multiplicity 1 had to be reduced from 3.5% to 0.5%. The respective data for the natural samarium sample are

completely based on the experimental data as no other information on the multiplicity distribution was available.

The correction of $\Sigma E$ for isotopic impurities assumed that the sum-energy spectrum of $^{151}$Sm can be approximated by a straight line in the energy range between 2 MeV and 7 MeV as illustrated in Figs. 3, 4. Corrections of 3.9%, 4.1%, and 3.7% were obtained for runs I to III, respectively. According to the above estimates the average correction of 3.9% is mostly due to the 3% contribution of $^{151}$Eu, while the parts of the even and odd samarium isotopes were found to be 0.9% and 0.8% only. The resulting total correction of 4.7% was used in the analysis of all runs.

The quantity $m$ in equation (1) denotes the sample thickness in atoms/b. The factor $F_1 = [100 - f(Au)]/[100 - f(X)]$ is used to correct for the fraction of capture events $f$ below the experimental threshold in sum energy, where $X$ refers to the respective samarium sample (Table 7), and $F_2$ is the ratio of the multiple scattering and self–shielding corrections.

The fraction of unobserved capture events, $f$, and the correction factor $F_1$ were calculated as described in Ref. [21]. The input for this calculation are the individual neutron capture cascades and their relative contributions to the total capture cross section as well as the detector efficiency for monoenergetic $\gamma$-rays in the energy range up to 10 MeV. As in the experiment on dysprosium [22] this information was derived directly from the experimental data recorded with the ADC system in run III. From these data, only events close to the sum energy peak (see Fig. 6) were selected, which contained the full capture $\gamma$-ray cascade. This ensemble was further reduced by restricting the analysis to the TOF region with optimum signal-to-background ratio (vertical lines in Fig. 5). The correction factors $F_1$ are quoted in Table 7.

The capture $\gamma$-ray spectra for the $^{151}$Sm and the $^{197}$Au sample obtained from the data taken with the ADC system are shown in Fig. 8 in energy bins of 500 keV. The $^{151}$Sm spectrum is significantly softer than the one of the gold sample.

The correction for neutron multiple scattering and self-shielding was calculated with the SESH code [17]. Apart from the pairing energies [23] most of the input parameters for the $^{151}$Sm sample were taken from Ref. [24]. Missing values were adopted from the calculation for $^{149}$Sm in Ref. [6], but slightly modified in order to reproduce the measured capture cross section. For the natural samarium sample the parameters from the previous measurement were used for all isotopes. For completeness the data for the gold sample are included since they differ slightly from the values used in Ref. [6] due to a revision of the total gold cross section. The final parameters are listed in Table 8 together with the calculated total cross sections. The resulting correction factors, MS(X) and $F_2$, are compiled in Table 9. In general, these corrections are smaller than 2%.

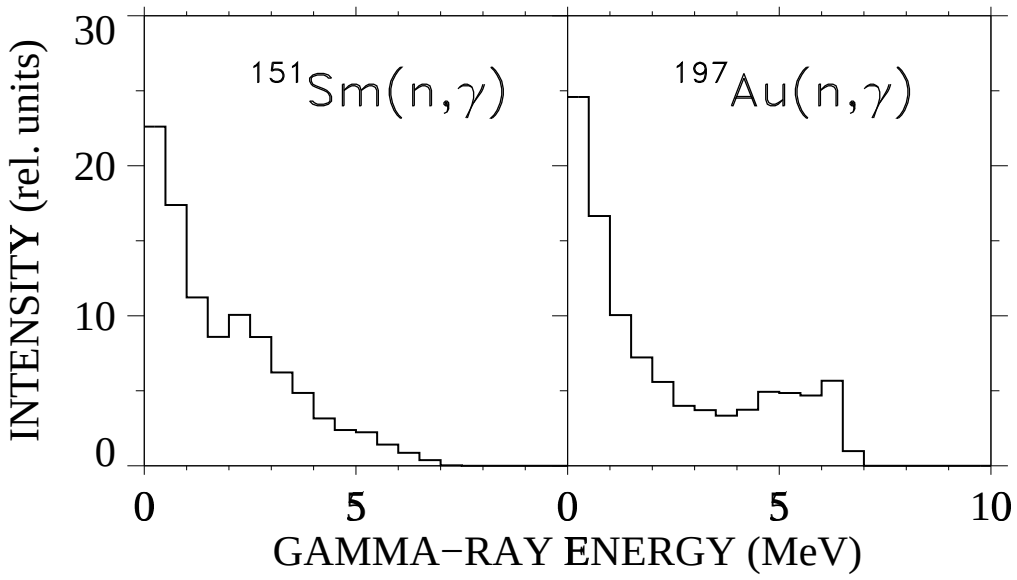


Figure 8: Capture $\gamma$-ray spectra derived from the capture cascades recorded with the ADC system. (The full resolution of 2048 channels is compressed into bins of 500 keV.)

Table 7: FRACTION OF UNDETECTED CAPTURE EVENTS, f (%), AND THE RELATED CORRECTION FACTORS $F_1$.

| | Threshold in Sum Energy (MeV) | | | |
|---|---|---|---|---|
| | 1.5 | 1.7 | 1.8 | 2.0 |
| f(Au) | 5.14 | 5.90 | 6.29 | 7.05 |
| f($^{151}$Sm) | 0.84 | 1.08 | 1.20 | 1.44 |
| f($^{nat}$Sm) | 2.22 | 2.86 | 3.18 | 3.82 |
| $F_1$($^{151}$Sm/Au) | 0.957 | 0.951 | 0.949 | 0.943 |
| $F_1$($^{nat}$Sm/Au) | 0.970 | 0.969 | 0.968 | 0.966 |

Table 8: PARAMETERS FOR THE CALCULATION OF NEUTRON SELF–SHIELDING AND MULTIPLE SCATTERING CORRECTIONS

| Parameter | | $^{151}$Sm | $^{197}$Au | $^{16}$O |
|---|---|---|---|---|
| Nucleon Number | | 151 | 197 | 16 |
| Binding Energy (MeV) | | 8.258 | 6.513 | 4.144 |
| Pairing Energy (MeV) | | 2.32 | 0.0 | 0.0 |
| Effective Temperature (K) | | 293 | 293 | 293 |
| Nuclear Spin | | 2.5 | 1.5 | 0 |
| Average Radiation | s | 0.092 | 0.128 | 0 |
| Width (eV) | p | 0.060 | 0.048 | |
| | d | 0.006 | 0.048 | |
| Average Level | s | 1.2 | 16.5 | 0 |
| Spacing (eV) | p[a] | 0.6 | 8.25 | |
| | d[a] | 0.4 | 5.28 | |
| Strength Function | $S_0$ | 4.2 | 2.0 | 0 |
| ($10^{-4}$) | $S_1$ | 0.5 | 0.4 | |
| | $S_2$ | 1.5 | 0.7 | |
| Nuclear Radius | s | 8.3 | 9.5 | 5.5 |
| (fm) | p | 8.3 | 9.5 | |
| | d | 8.3 | 9.5 | |
| | Calculated total cross sections | | | |
| 3 keV | | 39.9 | 26.1 | 3.80 |
| 5 keV | | 32.5 | 22.6 | 3.80 |
| 10 keV | | 25.0 | 18.9 | 3.79 |
| 20 keV | | 19.4 | 16.1 | 3.77 |
| 40 keV | | 15.1 | 13.8 | 3.74 |
| 80 keV | | 11.6 | 11.7 | 3.68 |
| 160 keV | | 8.6 | 9.6 | 3.55 |
| 320 keV | | 6.1 | 7.6 | 3.31 |

[a]Calculated with SESH [17]

Table 9: CORRECTION FACTORS FOR NEUTRON SELF–SHIELDING AND MULTIPLE SCATTERING, MS AND CORRECTION FACTORS FOR THE CROSS SECTION RATIOS, $F_2$ = MS(Au)/MS(X)

| Energy Bin | MS | | | $F_2$ | |
|---|---|---|---|---|---|
| (keV) | $^{197}$Au | $^{151}$Sm | $^{nat}$Sm | $^{151}$Sm/Au | $^{nat}$Sm/Au |
| 3 – 5 | 0.992 | 1.014 | 1.028 | 0.978 | 0.965 |
| 5 – 7.5 | 1.013 | 1.016 | 1.028 | 0.997 | 0.985 |
| 7.5 – 10 | 1.023 | 1.016 | 1.026 | 1.007 | 0.997 |
| 10 – 12.5 | 1.028 | 1.016 | 1.025 | 1.012 | 1.003 |
| 12.5 –15 | 1.031 | 1.016 | 1.024 | 1.014 | 1.007 |

Table 8 (continued)

| | | | | | |
|---|---|---|---|---|---|
| 15 – 20 | 1.033 | 1.016 | 1.023 | 1.017 | 1.010 |
| 20 – 25 | 1.033 | 1.016 | 1.022 | 1.017 | 1.011 |
| 25 – 30 | 1.032 | 1.015 | 1.021 | 1.017 | 1.011 |
| 30 – 40 | 1.031 | 1.015 | 1.020 | 1.016 | 1.011 |
| 40 – 50 | 1.031 | 1.014 | 1.019 | 1.017 | 1.012 |
| 50 – 60 | 1.030 | 1.013 | 1.018 | 1.016 | 1.012 |
| 60 – 80 | 1.029 | 1.013 | 1.016 | 1.016 | 1.013 |
| 80 – 100 | 1.028 | 1.012 | 1.015 | 1.016 | 1.013 |
| 100 – 120 | 1.027 | 1.011 | 1.015 | 1.016 | 1.012 |
| 120 – 150 | 1.026 | 1.011 | 1.014 | 1.015 | 1.012 |
| 150 – 175 | 1.025 | 1.010 | 1.014 | 1.015 | 1.011 |
| 175 – 200 | 1.024 | 1.010 | 1.013 | 1.014 | 1.011 |
| 200 – 225 | 1.023 | 1.010 | 1.013 | 1.013 | 1.010 |
| Uncertainty (%) | 0.3 | 0.1 | 0.2 | 0.3 | 0.4 |

# 4 GEANT SIMULATIONS

Additional information on the shape of the capture $\gamma$-ray spectra and on the multiplicity distribution was used in the present analysis. This information was obtained by a theoretical description of the neutron capture cascades based on the available information on the relevant level schemes. These cascades were used as input for a complete simulation of the experiment with the GEANT [25] code. This technique has been demonstrated to reproduce the measured sum energy spectra and multiplicity distributions quantitatively [26, 2].

The $\gamma$-ray cascades from neutron capture reactions on $^{151}$Sm isotope and on the $^{197}$Au standard were calculated using the CASINO [27] version of the Monte Carlo code DICEBOX [28], which is particularly suited for keV neutron energies. For the GEANT simulations described below, the proper treatment of the probability for emission of conversion electrons is an important feature of this code. Each of the simulations was carried out with a set of about 200000 neutron capture cascades. Within the individual cascades each step is marked to distinguish $\gamma$-ray transitions from transitions due to conversion electrons.

The experimental sum-energy spectrum of $^{151}$Sm is found consistent with the level scheme of $^{152}$Sm [30], which includes only levels with sufficiently short lifetimes to ensure that the complete capture cascade is detected in the 10 ns time window defined by the data acquisition system. In particular, there are no isomers, which could modify the sum energy spectrum in a way that could possibly be misinterpreted as an isotopic impurity. Examples of this type were recently identified in the hafnium isotopes [29].

For the present simulations the GEANT data base was complemented by the most recent neutron and gamma cross sections. The complex geometry of the Karlsruhe $4\pi$ $BaF_2$ detector was modeled for all 41 crystals including reflectors, photomultipliers, and

all structural materials. The efficiency for $\gamma$-rays originating from a sample in the center of the detector was then calculated including the effect of $\gamma$-ray self absorption. Converted $\gamma$-transitions were properly considered. Since conversion electrons are easily absorbed and do not contribute to the scintillation signal in the barium fluoride crystals this effect is important for the correct description of sum energy spectra. The energy resolution of the individual crystals was taken into account by using the values measured with calibrated sources.

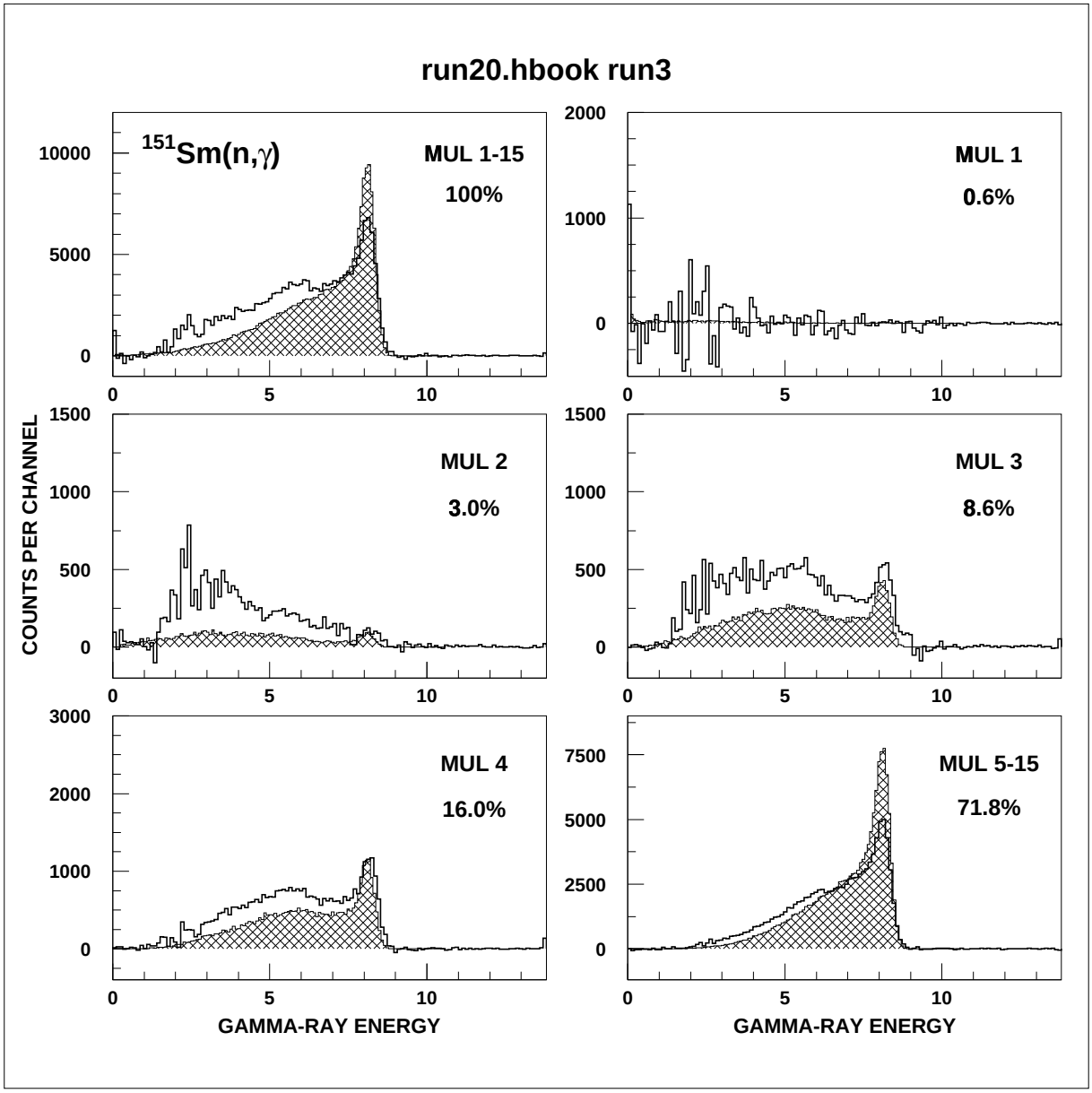


Figure 9: The dependence of sum-energy spectra on multiplicity for neutron capture in $^{151}$Sm. Simulated spectra (hatched areas) are compared with the experimental spectra of Fig 7 (histograms).

Yhe calculated neutron capture cascades were used to determine the response of the

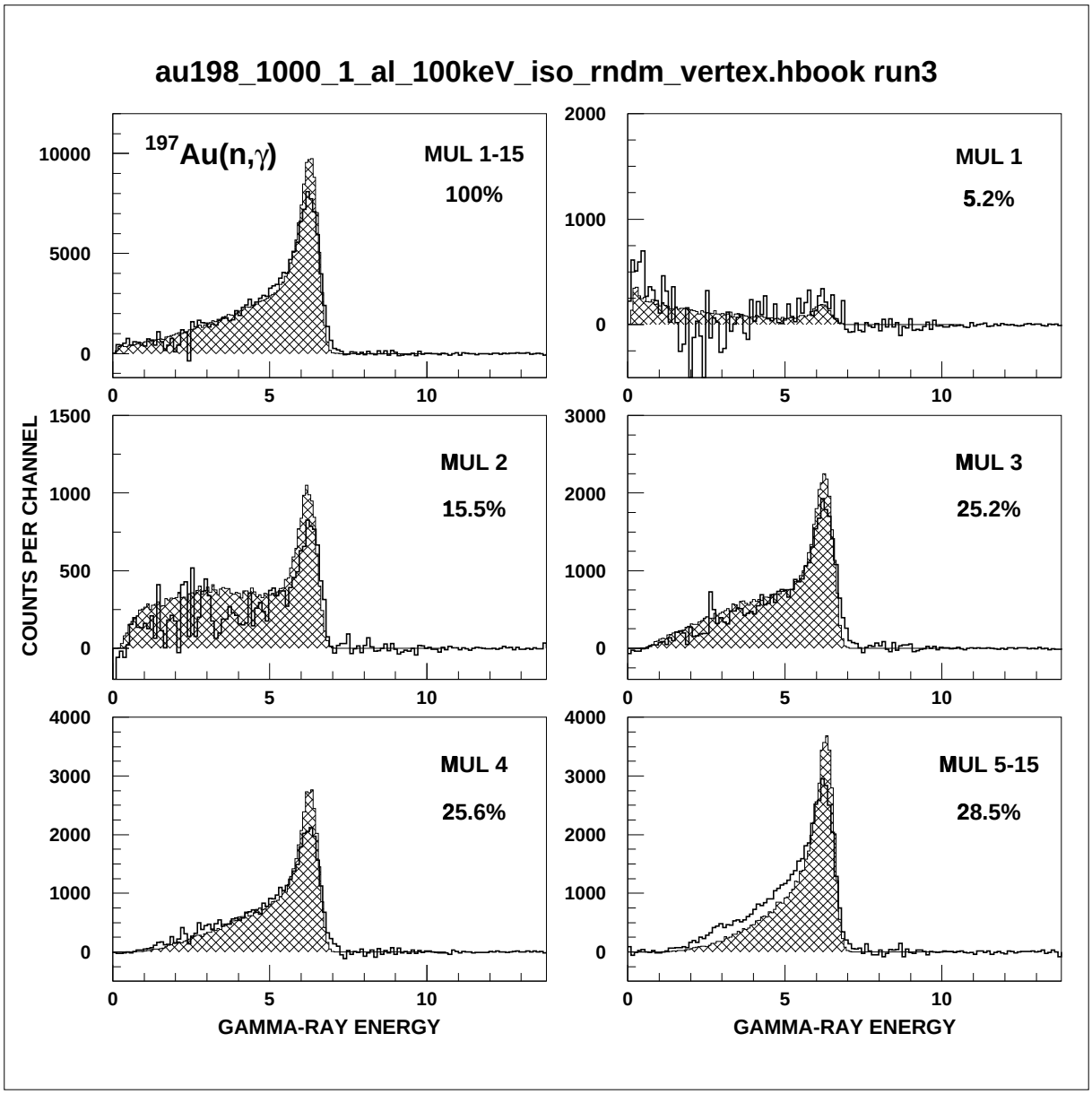


Figure 10: Same comparison as Fig. 9 for neutron capture in $^{197}$Au.

$4\pi$ $BaF_2$ detector by means of the GEANT simulations. For each cascade the $\gamma$-rays or electrons of the individual transitions were started in random directions at a common point inside the sample. The starting points were isotropically distributed over the volume of the sample and the deposited energy in the various detector modules was followed down to the experimental threshold of $\approx$50 keV.

Since each capture cascade was simulated separately, the spectra of the individual crystals and also the sum energy spectra could be stored as a function of multiplicity. As defined in Section 3, the multiplicity of an event is given by the total number of crystals, which registered an energy signal above 50 keV. The total recorded energy (sum energy) of this cascade was then stored in the respective multiplicity spectrum. Events were found

with multiplicities between 1 and 15, but with strongly decreasing probability above multiplicities of about 6. These simulated spectra are compared with the experimental results of Fig 7 in Figs. 9 and 10. In the upper left corner of Figs. 9 and 10 the total sum of all multiplicities is given, whereas the other five spectra correspond to the data shown in Fig. 7. It is important to note that the simulated spectra are only normalized via the total number of measured events.

The comparison of the measured and simulated spectra show surprisingly good agreement with respect to the sum energy peak at the binding energy of the captured neutron as well as for the tail towards lower energies, although this tail shows large statistical fluctuations in the experimental spectra with multiplicities 1 and 2 because of the large backgrounds in this region. Nevertheless, the multiplicity distribution is well reproduced if one compares the relative contributions to the respective numbers given in Fig. 7. However, the shape of the full energy peaks of $^{151}$Sm and $^{197}$Au could not be reproduced as well as in previous simulations for $^{181}$Ta [3] and for the xenon isotopes [2]. This problem may result from the significant background below $\sim$ 200 keV due to the radioactivity of the sample, which could have affected the stabilization of the crystals over the long measuring times of the present experiment.

Table 10: FRACTION OF UNDETECTED CAPTURE EVENTS, f (in %), AND THE RELATED CORRECTION FACTORS $F_1$.[a]

| | Threshold in Sum Energy (MeV) | | | |
|---|---|---|---|---|
| | 1.5 | 1.7 | 1.8 | 2.0 |
| f(Au) | 4.19 | 5.19 | 5.68 | 6.68 |
| f($^{151}$Sm) | 0.55 | 0.75 | 0.86 | 1.06 |
| $F_1$($^{151}$Sm/Au) | 0.963 | 0.955 | 0.951 | 0.943 |

[a] derived from the GEANT simulations

The simulations are important as they provide an independent check of the correction for the fraction of capture events, which escaped detection. This correction contributes significantly to the overall systematic uncertainty of the final cross section. The respective spectrum fractions $f$ below sum energy thresholds of 1.5 MeV and 2 MeV were deduced from the simulated spectra in the upper left corner of Figs. 9 and 10 and are listed in Table 10 together with the corresponding correction factors $F_1$ for the cross section ratio relative to the gold standard. At the actual experimental threshold energies of 1.7 and 1.8 MeV the simulated results for $F_1$ agree with the values obtained from the experimentally measured cascades (Table 7) within 0.3% on average. This agreement between the independently determined corrections confirms the uncertainties assigned to this correction.

# 5 DIFFERENTIAL NEUTRON CAPTURE CROSS SECTIONS

The measured neutron capture cross section ratios of the investigated Sm isotopes and of $^{197}$Au are listed in Tables 11 and 12 together with the respective statistical uncertainties. The data are given for all runs and for the two evaluation methods discussed in Sec. 3. The last column in each table contains the weighted average, the weight being determined by the inverse of the squared statistical uncertainties. Since the cross section ratios depend weakly on energy, the averages for the energy interval from 30 to 80 keV are also included for a better comparison of the individual results. The data are free of systematic differences with respect to the various runs and evaluations and well consistent within the quoted statistical uncertainties. The largest deviation of about $3\sigma$ was found for $^{151}$Sm, where the evaluation 1 of run II yields a value, which exceeds the quoted average by 7.4%, while all other values agree within $2\sigma$. Even for natural samarium, where the statistical uncertainties are systematically larger due to the five times smaller cross section, all deviations are well below $1\sigma$.

As in previous studies with the $4\pi$ $BaF_2$ detector [6, 14, 31], the final cross section ratios were adopted from evaluation 2. The respective mean values are compiled in Table 13 together with the statistical, systematic, and total uncertainties. The energy bins are sufficiently fine to avoid systematic effects in calculating the Maxwellian averaged cross section (Sec. 7). In the energy bins from 15 to 200 keV statistical uncertainties below 2.0% and 4% could be obtained for for the $^{151}$Sm for the natural samarium sample, respectively. The corresponding systematic uncertainties are 1.9 and 0.6%.

The experimental ratios were converted into absolute cross sections using the gold data of Macklin [32] normalized by a factor of 0.989 to the absolute value of Ratynski and Käppeler [33] (Table 14). The uncertainties of the resulting values can be obtained by adding the 1.5% uncertainty of the reference cross section to the uncertainties of the respective cross section ratios.

The energy dependence of the present results are shown in Fig. 11. A comparison of the capture cross section of $^{151}$Sm with the results of the n_TOF collaboration is pending since no final data have been released yet. Experimental information for elemental samarium is very scarce. Therefore, the data shown in Fig. 11 were evaluated using the cross sections of the five isotopes, which were measured with the Karlsruhe $4\pi BaF_2$ detector [6]. For the missing isotopes the $^{144}$Sm cross section from the evaluation of Kopecky *et al.* [34] was normalized by using the ratio to the experimental data of $^{147}$Sm and $^{148}$Sm from Ref. [6]. The $^{154}$Sm was normalized as to match the Maxwellian averaged cross section at kT=30 keV with the result of a recent activation experiment [9]. Given the present experimental uncertainties and the relatively crude evaluation the overall good agreement is satisfactory. Cross sections reported from measurements by Kononov *et al.* [35] and by Gibbons *et al.* [36] are higher by factors of up to 2 compared to the present results and were, therefore, not included in the comparison.

With respect to Fig. 11 note that in the energy interval between 7.5 keV and 10 keV both cross sections appear to be systematically lower than a smooth trend would suggest.

Table 11: $\sigma(^{151}\mathrm{Sm})/\sigma(^{197}\mathrm{Au})$ AND STATISTICAL UNCERTAINTIES (in %)

| Energy Bin (keV) | Run I | | Run II | | Run III | | Average | |
|---|---|---|---|---|---|---|---|---|
| evaluation 1 | | | | | | | | |
| 3 – 5 | 1.9510 | 20. | 10.3150 | 19. | 11.4553 | 39. | 6.7825 | 15. |
| 5 – 7.5 | 2.8302 | 12. | 8.3971 | 14. | 6.4922 | 15. | 5.5789 | 8.6 |
| 7.5 – 10 | 3.4677 | 9.2 | 8.5375 | 15. | 5.0893 | 10. | 4.9443 | 6.6 |
| 10 – 12.5 | 5.2338 | 6.8 | 8.5525 | 12. | 5.0900 | 7.6 | 5.7088 | 4.8 |
| 12.5 – 15 | 5.2591 | 6.1 | 8.0605 | 10. | 5.8295 | 6.9 | 5.9504 | 4.2 |
| 15 – 20 | 4.5572 | 3.7 | 6.0662 | 5.3 | 5.8316 | 4.0 | 5.3338 | 2.4 |
| 20 – 25 | 5.6161 | 3.1 | 6.1133 | 4.8 | 6.0093 | 3.4 | 5.8499 | 2.1 |
| 25 – 30 | 5.2988 | 2.6 | 6.1822 | 4.0 | 5.5650 | 2.8 | 5.5658 | 1.7 |
| 30 – 40 | 5.6877 | 2.1 | 6.2985 | 3.0 | 5.4815 | 2.4 | 5.7448 | 1.4 |
| 40 – 50 | 5.4370 | 2.1 | 6.0692 | 3.1 | 5.4550 | 2.4 | 5.5718 | 1.4 |
| 50 – 60 | 5.6092 | 2.0 | 5.7863 | 3.0 | 5.3386 | 2.3 | 5.5501 | 1.4 |
| 60 – 80 | 5.0358 | 1.8 | 5.4242 | 2.6 | 4.9346 | 2.1 | 5.0871 | 1.2 |
| 80 – 100 | 4.7707 | 1.9 | 4.8516 | 2.6 | 4.3921 | 2.3 | 4.6713 | 1.3 |
| 100 – 120 | 4.4080 | 2.0 | 4.2959 | 2.7 | 4.2129 | 2.3 | 4.3165 | 1.3 |
| 120 – 150 | – | – | 3.9760 | 2.6 | – | – | 3.9760 | 2.6 |
| 150 – 175 | – | – | 3.7948 | 2.7 | – | – | 3.7948 | 2.7 |
| 175 – 200 | – | – | 3.3823 | 3.0 | – | – | 3.3823 | 3.0 |
| 200 – 225 | – | – | 3.3320 | 5.3 | – | – | 3.3320 | 5.3 |
| 30 – 80 | 5.4424 | 1.6 | 5.8946 | 2.0 | 5.3024 | 1.6 | 5.4885 | 1.1 |
| evaluation 2 | | | | | | | | |
| 3 – 5 | 0.8239 | 36. | 3.1254 | 21. | 9.3920 | 23. | 5.1766 | 17. |
| 5 – 7.5 | 2.2357 | 12. | 4.5126 | 14. | 6.1955 | 11. | 4.5172 | 7.5 |
| 7.5 – 10 | 2.8068 | 8.6 | 5.6112 | 14. | 5.5518 | 7.9 | 4.4857 | 5.6 |
| 10 – 12.5 | 4.7628 | 6.2 | 6.5203 | 11. | 5.4927 | 5.9 | 5.3337 | 4.0 |
| 12.5 – 15 | 4.9035 | 5.4 | 6.9156 | 9.2 | 5.9982 | 5.3 | 5.6682 | 3.5 |
| 15 – 20 | 5.0702 | 3.1 | 5.8113 | 4.8 | 6.0400 | 3.2 | 5.5837 | 2.0 |
| 20 – 25 | 5.9317 | 2.6 | 6.2058 | 4.2 | 6.2477 | 2.7 | 6.1048 | 1.7 |
| 25 – 30 | 5.4810 | 2.3 | 5.8456 | 3.4 | 5.7632 | 2.3 | 5.6615 | 1.5 |
| 30 – 40 | 5.5653 | 1.8 | 5.8724 | 2.6 | 5.5471 | 1.9 | 5.6217 | 1.2 |
| 40 – 50 | 5.6008 | 1.8 | 5.9626 | 2.7 | 5.5232 | 1.9 | 5.6438 | 1.2 |
| 50 – 60 | 5.7180 | 1.8 | 5.7190 | 2.6 | 5.4259 | 1.9 | 5.6083 | 1.2 |
| 60 – 80 | 5.1412 | 1.6 | 5.3687 | 2.2 | 4.9295 | 1.7 | 5.1157 | 1.1 |
| 80 – 100 | 4.8566 | 1.7 | 4.8136 | 2.2 | 4.4350 | 1.8 | 4.7008 | 1.1 |
| 100 – 120 | 4.4585 | 1.8 | 4.2701 | 2.3 | 4.1596 | 1.9 | 4.3067 | 1.1 |
| 120 – 150 | – | – | 3.9689 | 2.1 | – | – | 3.9689 | 2.1 |
| 150 – 175 | – | – | 3.7748 | 2.3 | – | – | 3.7748 | 2.3 |
| 175 – 200 | – | – | 3.3679 | 2.5 | – | – | 3.3679 | 2.5 |
| 200 – 225 | – | – | 3.1516 | 4.3 | – | – | 3.1516 | 4.3 |
| 30 – 80 | 5.5063 | 1.4 | 5.7307 | 1.6 | 5.3564 | 1.6 | 5.4974 | 0.9 |

Table 12: $\sigma(^{nat}\mathrm{Sm})/\sigma(^{197}\mathrm{Au})$ AND STATISTICAL UNCERTAINTIES (in %)

| Energy Bin (keV) | Run I | | Run II | | Run III | | Average | |
|---|---|---|---|---|---|---|---|---|
| evaluation 1 | | | | | | | | |
| 7.5 – 10 | – | – | – | – | 0.4439 | 47. | 0.4439 | 47. |
| 10 – 12.5 | – | – | – | – | 0.6630 | 23. | 0.6630 | 23. |
| 12.5 – 15 | 0.4525 | 29. | 0.3535 | 77. | 0.8462 | 17. | 0.7254 | 15. |
| 15 – 20 | 0.7572 | 9.3 | 0.7450 | 17. | 0.9549 | 9.3 | 0.8423 | 6.2 |
| 20 – 25 | 1.1000 | 6.1 | 1.0502 | 11. | 1.0642 | 7.5 | 1.0801 | 4.4 |
| 25 – 30 | 0.9609 | 5.5 | 0.9737 | 9.5 | 0.9375 | 6.7 | 0.9550 | 3.9 |
| 30 – 40 | 0.9236 | 4.4 | 0.8198 | 7.9 | 0.8845 | 5.8 | 0.8947 | 3.2 |
| 40 – 50 | 1.0355 | 4.1 | 0.9925 | 6.9 | 0.9186 | 5.7 | 0.9948 | 3.0 |
| 50 – 60 | 1.0853 | 3.9 | 1.0430 | 6.4 | 1.0253 | 5.4 | 1.0607 | 2.8 |
| 60 – 80 | 1.0154 | 3.5 | 1.0121 | 5.4 | 0.9868 | 5.2 | 1.0078 | 2.6 |
| 80 – 100 | 1.0752 | 3.5 | 1.0090 | 5.2 | 1.0099 | 5.2 | 1.0438 | 2.6 |
| 100 – 120 | 1.0704 | 3.8 | 0.9994 | 5.2 | 0.9373 | 5.4 | 1.0194 | 2.7 |
| 120 – 150 | – | – | 0.9883 | 4.9 | – | – | 0.9883 | 4.9 |
| 150 – 175 | – | – | 1.0416 | 5.1 | – | – | 1.0416 | 5.1 |
| 175 – 200 | – | – | 0.9644 | 5.6 | – | – | 0.9644 | 5.6 |
| 200 – 225 | – | – | 1.0925 | 9.3 | – | – | 1.0925 | 9.3 |
| 30 – 80 | 1.0150 | 3.1 | 0.9669 | 3.7 | 0.9538 | 4.9 | 0.9895 | 2.1 |
| evaluation 2 | | | | | | | | |
| 3 – 5 | – | – | – | – | 0.8869 | 56. | 0.8869 | 56. |
| 5 – 7.5 | 0.4570 | 35. | 0.9603 | 32. | 1.0329 | 21. | 0.8985 | 16. |
| 7.5 – 10 | 0.5608 | 24. | 0.3884 | 86. | 0.9689 | 17. | 0.8234 | 14. |
| 10 – 12.5 | 0.4671 | 27. | 0.3721 | 71. | 1.1026 | 11. | 0.9985 | 10. |
| 12.5 – 15 | 0.7683 | 14. | 0.6403 | 35. | 1.1264 | 10. | 0.9908 | 8.1 |
| 15 – 20 | 0.8243 | 7.4 | 0.9146 | 12. | 1.0479 | 6.4 | 0.9469 | 4.5 |
| 20 – 25 | 1.0664 | 5.3 | 1.2641 | 8.1 | 1.1334 | 5.2 | 1.1289 | 3.4 |
| 25 – 30 | 1.0178 | 4.5 | 1.0933 | 7.1 | 0.9679 | 4.7 | 1.0112 | 3.0 |
| 30 – 40 | 0.9844 | 3.6 | 0.8857 | 6.1 | 0.9155 | 4.1 | 0.9429 | 2.5 |
| 40 – 50 | 1.0521 | 3.5 | 1.0555 | 5.5 | 0.9436 | 4.0 | 1.0150 | 2.4 |
| 50 – 60 | 1.0746 | 3.3 | 1.0895 | 5.1 | 1.0151 | 3.9 | 1.0572 | 2.3 |
| 60 – 80 | 0.9999 | 3.0 | 1.0481 | 4.4 | 0.9653 | 3.7 | 0.9998 | 2.1 |
| 80 – 100 | 1.0425 | 3.0 | 1.0419 | 4.2 | 1.0127 | 3.7 | 1.0333 | 2.1 |
| 100 – 120 | 1.0307 | 3.2 | 1.0125 | 4.3 | 0.9357 | 3.8 | 0.9961 | 2.1 |
| 120 – 150 | – | – | 0.9967 | 4.0 | – | – | 0.9967 | 4.0 |
| 150 – 175 | – | – | 0.9955 | 4.3 | – | – | 0.9955 | 4.3 |
| 175 – 200 | – | – | 0.9543 | 4.6 | – | – | 0.9543 | 4.6 |
| 200 – 225 | – | – | 0.9553 | 8.0 | – | – | 0.9553 | 8.0 |
| 30 – 80 | 1.0278 | 2.7 | 1.0197 | 3.1 | 0.9599 | 3.4 | 1.0037 | 1.7 |

Table 13: FINAL NEUTRON CAPTURE CROSS SECTION RATIOS OF $^{151}$Sm AND $^{nat}$Sm RELATIVE TO $^{197}$Au

| Energy Bin[a] | $\frac{\sigma(^{151}Sm)}{\sigma(^{197}Au)}$ | Uncertainty (%) | | | $\frac{\sigma(^{nat}Sm)}{\sigma(^{197}Au)}$ | Uncertainty (%) | | |
|---|---|---|---|---|---|---|---|---|
| (keV) | | stat | sys | tot | | stat | sys | tot |
| 3 – 5 | 5.1766 | 17. | 1.9 | 17. | 0.8869 | 56. | 0.6 | 56. |
| 5 – 7.5 | 4.5172 | 7.5 | 1.9 | 7.7 | 0.8985 | 16. | 0.6 | 16. |
| 7.5 – 10 | 4.4857 | 5.6 | 1.9 | 5.9 | 0.8234 | 14. | 0.6 | 14. |
| 10 – 12.5 | 5.3337 | 4.0 | 1.9 | 4.4 | 0.9985 | 10. | 0.6 | 10. |
| 12.5 – 15 | 5.6682 | 3.5 | 1.9 | 4.0 | 0.9908 | 8.1 | 0.6 | 8.1 |
| 15 – 20 | 5.5837 | 2.0 | 1.9 | 2.8 | 0.9469 | 4.5 | 0.6 | 4.5 |
| 20 – 25 | 6.1048 | 1.7 | 1.9 | 2.5 | 1.1289 | 3.4 | 0.6 | 3.5 |
| 25 – 30 | 5.6615 | 1.5 | 1.9 | 2.4 | 1.0112 | 3.0 | 0.6 | 3.1 |
| 30 – 40 | 5.6217 | 1.2 | 1.9 | 2.2 | 0.9429 | 2.5 | 0.6 | 2.6 |
| 40 – 50 | 5.6438 | 1.2 | 1.9 | 2.2 | 1.0150 | 2.4 | 0.6 | 2.5 |
| 50 – 60 | 5.6083 | 1.2 | 1.9 | 2.2 | 1.0572 | 2.3 | 0.6 | 2.4 |
| 60 – 80 | 5.1157 | 1.1 | 1.9 | 2.2 | 0.9998 | 2.1 | 0.6 | 2.2 |
| 80 – 100 | 4.7008 | 1.1 | 1.9 | 2.2 | 1.0333 | 2.1 | 0.6 | 2.2 |
| 100 – 120 | 4.3067 | 1.1 | 1.9 | 2.2 | 0.9961 | 2.1 | 0.6 | 2.2 |
| 120 – 150 | 3.9689 | 2.1 | 1.9 | 2.8 | 0.9967 | 4.0 | 0.6 | 4.0 |
| 150 – 175 | 3.7748 | 2.3 | 1.9 | 3.0 | 0.9955 | 4.3 | 0.6 | 4.3 |
| 175 – 200 | 3.3679 | 2.5 | 1.9 | 3.1 | 0.9543 | 4.6 | 0.6 | 4.6 |
| 200 – 225 | 3.1516 | 4.3 | 1.9 | 4.7 | 0.9553 | 8.0 | 0.6 | 8.0 |

[a] Energy bins as used for calculating the Maxwellian averaged cross sections

# 6 DISCUSSION OF UNCERTAINTIES

The determination of statistical and systematic uncertainties followed the procedures applied in previous measurements with the $4\pi$ $BaF_2$ detector [6, 14]. Therefore, a discussion of the particular aspects of the present experiment may suffice here. The various contributions to the overall uncertainties are compiled in Table 15.

The binding energy for the samarium isotopes is sufficiently low that the scattering background could be normalized in the sum energy region around 9 MeV and reliably subtracted. The resulting data from individual runs or related to the different acquisition modes and evaluation methods were free of systematic differences (see Tables 11 and 12). The only exception found was the result for $^{151}$Sm obtained in evaluation 1 of run II (Sec.5). Accordingly, systematic uncertainties in background subtraction were negligible as in the measurements on samarium [6], gadolinium [7], and dysprosium [22].

In contrast to previous experiments the count rate of the individual detector modules differed significantly due to the radioactivity of the sample. Though the low Q-value for $\beta^-$decay is only 76.8 keV the background in the crystals extends up to ~200 keV before

Table 14: NEUTRON CAPTURE CROSS SECTIONS OF $^{151}$Sm, AND $^{nat}$Sm (in mb).

| Energy Bin (keV) | $\sigma(^{197}\mathrm{Au})^a$ | $\sigma(^{151}\mathrm{Sm})$ | $\sigma(^{nat}\mathrm{Sm})$ |
|---|---|---|---|
| 3 – 5 | 2266.7 | 11734. | 2010. |
| 5 – 7.5 | 1726.7 | 7800. | 1552. |
| 7.5 – 10 | 1215.7 | 5454. | 1001. |
| 10 – 12.5 | 1066.7 | 5690. | 1065. |
| 12.5 – 15 | 878.0 | 4977. | 869.9 |
| 15 – 20 | 738.8 | 4125. | 699.5 |
| 20 – 25 | 600.0 | 3663. | 677.4 |
| 25 – 30 | 570.8 | 3231. | 577.2 |
| 30 – 40 | 500.4 | 2813. | 471.8 |
| 40 – 50 | 433.3 | 2446. | 439.8 |
| 50 – 60 | 389.6 | 2185. | 411.9 |
| 60 – 80 | 349.4 | 1787. | 349.3 |
| 80 – 100 | 298.3 | 1402. | 308.2 |
| 100 – 120 | 290.1 | 1250. | 289.0 |
| 120 – 150 | 274.1 | 1088. | 273.2 |
| 150 – 175 | 263.7 | 995.2 | 262.5 |
| 175 – 200 | 252.6 | 850.6 | 241.0 |
| 200 – 225 | 248.5 | 783.0 | 237.4 |

[a]Based on the $^{197}$Au data discussed in text

it strongly decreases. The average count rate of the individual detector modules is 1550 $s^{-1}$, but reached 2700 $s^{-1}$ in the runs with $\sim 2\mu$A proton beam current on target. With the $^{151}$Sm source mounted in the center of the detector the count rate increased to 12600 $s^{-1}$ on average with peak values of 13400 and 14600 $s^{-1}$ in runs with 100 and 225 keV maximum neutron energy, respectively. During the entire experiment the discriminator threshold of the timing signals was set at 50 keV. During the periodical checks of the proper setting the $^{151}$Sm sample had to be removed from the detector. The background from the $^{151}$Sm decay was equally distributed in the individual detector modules since it was only shifted by 4 cm to its out of beam position when the gold sample was measured. The nearly identical background obtained for both samples justified the assumption that the related systematic uncertainty in the measured cross section ratio was negligible.

The minor systematic uncertainties in Table 15 related to the flight path measurement and the neutron flux normalization have been discussed before.

The correction for the change in sample mass due to the decay of $^{151}$Sm required to consider the uncertainty of the half life. The actual $^{151}$Sm mass at the time of the measurements was determined from the 93 yr half life given by the Karlsruhe chart of the nuclides, which corresponds to the value of $t_{1/2}$=93±8 yr of Reynolds *et al.* [37]. The latest compilation recommends a value of $t_{1/2}$=90±8 yr [38], presumably an average between the results of Reynolds *et al.* and Flynn *et al.* [39] who reported a value of $t_{1/2}$=87±9 yr. However, the 8 yr uncertainty translates into a systematic uncertainty in the $^{151}$Sm mass of only 0.2% at the time of the measurement. The same uncertainty was

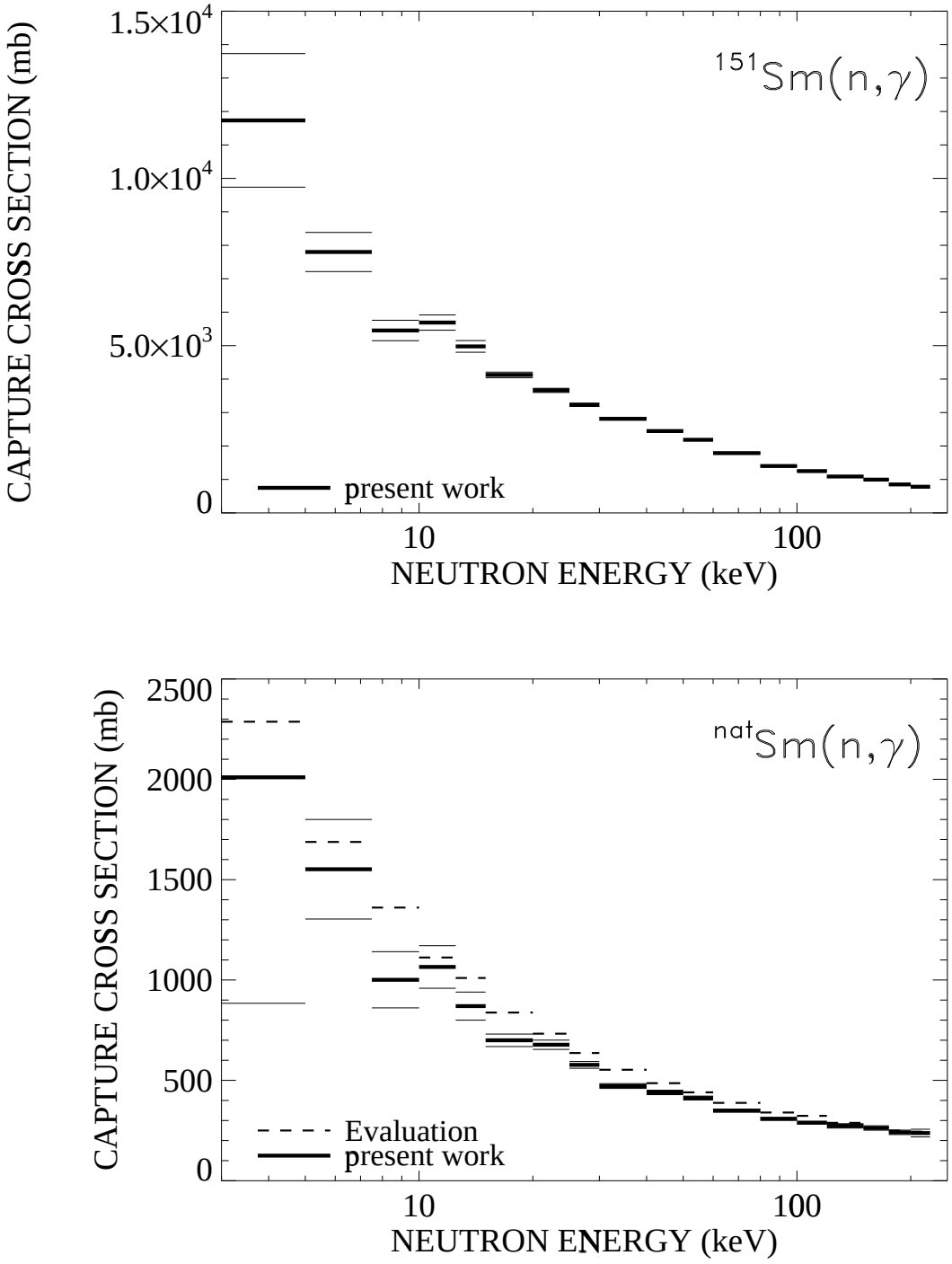


Figure 11: The neutron capture cross sections of $^{151}$Sm and of natural samarium. The latter data are compared to an evaluated cross section, which is essentially based on the data of Ref.[6] (see text).

also assumed for the mass of the natural samarium sample since elemental impurities on this level were recently found for a natural lutetium sample as well [29].

The isotopic composition of highly enriched samples is commonly specified with absolute uncertainties of 0.2%, which seems to be rather conservative compared to an independent determination for some neodymium isotopes [20]. Nevertheless, this value was adopted in the present $^{151}$Sm analysis as well.

The uncertainty of the isotopic correction requires special attention. As shown in Figs. 3 and 4 events above the straight line were eliminated for each run separately, yielding an average correction of 3.9%. The spread of the individual results (Sec. 3) was used to estimate a systematic uncertainty of 0.2%. However, only part of the correction was considered, namely those events in the energy range from 4.8 MeV to 6.6 MeV, whereas the low energy tail of the capture events was missed due to lack of statistics. For the even samarium isotopes it was estimated from Fig. 3 that about 30% of the events were not considered. Due to the higher binding energy of the europium isotopes the missed fraction is only 20% in this case. Since 3% of the correction are due to europium and 0.9% due to the even samarium isotopes, the respective contributions to the systematic uncertainty are 0.75 and 0.40%, respectively. Finally a fourth component of 0.2% was assumed for the contribution of the odd samarium isotopes. Altogether a systematic uncertainty of 1.6% was obtained for the isotopic correction of the $^{151}$Sm data.

The uncertainty for the correction of multiple scattering and self-shielding was adopted from the output file of the SESH code. The calculation of the correction factors MS was carried out for a pure $^{151}$Sm sample as well as for the actual sample including the isotopic impurities. The difference between both results was only $\approx$0.3%, independent of the neutron energy. In our previous experiments 25% of this difference was added to the uncertainty provided by the SESH code. In the present case, this additional component is negligible.

The detailed discussion of the systematic uncertainties due to undetected events for the gadolinium experiment [7] showed that uncertainties of the correction factor $F_1$ were 0.3% for the even and 0.8% for the odd isotopes. These corrections were based on two independent sets of calculated capture cascades, and were found to agree with the respective uncertainties quoted in previous measurements with the $4\pi$ $BaF_2$ detector [6, 14, 31]. It turned out that this uncertainty was mainly determined by the difference in binding energy between the investigated isotope and the gold standard, which is large for odd, but small for even isotopes. This result was verified with experimental $\gamma$-ray cascades from capture on various dysprosium isotopes [22] and confirmed the reliability of the evaluated uncertainties. With this procedure, uncertainties of 0.8% and 0.4% were obtained for the correction factors $F_1$ of the $^{151}$Sm sample and of the natural sample (effective binding energy 5.8 MeV), respectively. This uncertainty is confirmed by comparison with the independent determination of the correction $F_1$ in the GEANT simulations (Table 10).

Table 15: SYSTEMATIC UNCERTAINTIES (%)

| | |
|---|---|
| Flight path | 0.1 |
| Neutron flux normalization | 0.2 |
| Sample mass: elemental impurities | 0.2 |
| Isotopic composition ($^{151}$Sm only ) | 0.2 |
| Isotopic correction ($^{151}$Sm only ) | 1.6 |
| Multiple scattering and self–shielding: $F_2$ | |
| cross section ratio $^{151}$Sm/$^{nat}$Sm | 0.3/0.4 |
| Undetected events: $F_1$ | |
| cross section ratio $^{151}$Sm/$^{nat}$Sm | 0.8/0.4 |
| total systematic uncertainties | |
| $\sigma(^{151}\mathrm{Sm})/\sigma(\mathrm{Au})$ | 1.9 |
| $\sigma(^{nat}\mathrm{Sm})/\sigma(\mathrm{Au})$ | 0.6 |

# 7 MAXWELLIAN AVERAGED CROSS SECTIONS

Maxwellian averaged cross sections were calculated in the same way as described in Refs. [14, 21]. The neutron energy range from 0 - 700 keV was divided into three intervals $I_x$ according to the origin of the adopted cross sections (see Table 16). The dominant part $I_2$ between 3 keV and 225 keV is provided by the present experiment (Table 14). These data were obtained with sufficient resolution in neutron energy to exclude systematic uncertainties that may result in the calculation of the Maxwellian average if the energy grid is too coarse.

The contribution $I_1$ was determined by normalizing the cross sections of Kopecky *et al.* [34] to the present data in the interval between 3 keV and 50 keV. Since the shape of both data sets were found in good agreement, an uncertainty of 5% was assumed for the contribution $I_1$.

At typical *s*-process temperatures the energy interval from 225 keV to 700 keV contributes very little to the Maxwellian average. For this part, the data of Kopecky *et al.* [34] were normalized to the present results between 100 and 225 keV, and the corresponding uncertainties were assumed to increase from 2% at 225 keV to 10% at 700 keV.

The systematic uncertainties of the Maxwellian averaged cross sections in Table 16 are determined by the uncertainties of the measured cross section ratios in the interval $I_2$ (Table 13) as well as by the respective $I_1$ and $I_3$ contributions. The 1.5% uncertainty of the gold standard was not included since it cancels out in most applications of relevance for *s*-process studies. In general, the systematic uncertainties dominate over the statistical uncertainties, except at low thermal energies.

The present results at $kT$=30 keV are eventually compared in Table 17 with the result obtained by the n_TOF collaboration and with previous calculations quoted in the

compilations of Bao *et al.* [1] and of Beer, Voss, and Winters [43]. The present result is in excellent agreement with the n_TOF value [44] but significantly more accurate. It is surprising to see that the $^{151}$Sm cross section was systematically underestimated in all theoretical calculations.

Table 16: MAXWELLIAN AVERAGED NEUTRON CAPTURE CROSS SECTIONS OF $^{151}$Sm.

| $^{151}$Sm | | | | | | | |
|---|---|---|---|---|---|---|---|
| $\Delta$E | 0 - 3 keV | 3 - 225 keV | 225 - 700 keV | Thermal Spectrum | | | |
| Data: | from Ref. [34][a] | this work | from Ref. [34][a] | | | | |
| kT | $I_1$ | $I_2$ | $I_3$ | $<\sigma v>/v_T$ (mbarn) | | | |
| (keV) | (mbarn) | (mbarn) | (mbarn) | | stat | sys[b] | tot |
| 8 | 1384.±69. | 5644.±203. | 0.0 | 7028. | 214. | 133. | 252. |
| 10 | 923.4±46. | 5159.±150. | 0.0 | 6082. | 157. | 115. | 195. |
| 15 | 433.8±22. | 4270.±85. | 0.0 | 4704. | 88. | 89. | 125. |
| 20 | 251.0±13. | 3674.±58. | 0.1 | 3925. | 59. | 75. | 95. |
| 25 | 163.4±8.2 | 3243.±44. | 0.8 | 3407. | 45. | 65. | 79. |
| 30 | 114.7±5.7 | 2913.±35. | 3.1±0.1 | 3031. | 36. | 58. | 68. |
| 40 | 65.5±3.3 | 2429.±26. | 15.0±0.4 | 2510. | 26. | 48. | 55. |
| 50 | 42.3±2.1 | 2079.±21. | 36.6±1.0 | 2158. | 21. | 41. | 46. |
| 52 | 39.1±2.0 | 2020.±20. | 41.7±1.2 | 2101. | 20. | 40. | 45. |
| 60 | 29.5±1.5 | 1807.±18. | 83.8±2.5 | 1920. | 18. | 36. | 40. |
| 70 | 21.8±1.1 | 1586.±16. | 92.3±2.9 | 1700. | 16. | 32. | 36. |
| 80 | 16.7±0.8 | 1402.±14. | 119.3±3.9 | 1538. | 15. | 29. | 33. |
| 90 | 13.2±0.7 | 1248.±13. | 143.3±4.9 | 1405. | 14. | 27. | 30. |
| 100 | 10.8±0.5 | 1117.±11. | 163.6±5.7 | 1291. | 12. | 25. | 28. |

[a] Normalized to present data.
[b] The 1.5% uncertainty of the gold cross section is not included, since it cancels out in most applications of relevance for nuclear astrophysics.

Table 17: MAXWELLIAN AVERAGED CROSS SECTIONS OF $^{151}$Sm (in mb) AT $kT$=30 keV COMPARED TO PREVIOUS DATA

| Experiment | | Calculation | | Evaluation | |
|---|---|---|---|---|---|
| 3031 ± 68 | this work[a] | 1542 | [40] | 1932±206 | [43] |
| 3100 ± 160 | [44] | 1820 ± 460 | [8] | 2710±420 | [1] |
| | | 1932 | [5] | | |
| | | 2809 | [41] | | |
| | | 1990 | [42] | | |

[a]The 1.5% uncertainty of the gold cross section is not included, since it cancels out in most applications of relevance for nuclear astrophysics.

# 8 ACKNOWLEDGMENTS

We are indebted to G. Rupp for his invaluable technical assistance, which was essential for the success of this work.

# References

[1] Z.Y. Bao, H. Beer, F. Käppeler, F. Voss, K. Wisshak, and T. Rauscher, Atomic Data Nucl. Data Tables **76**, 70 (2000).

[2] R. Reifarth, M. Heil, F. Käppeler, F. Voss, K. Wisshak, F. Bečvář, M. Krtička, R. Gallino, Y. Nagai, Phys. Rev. C **66**, 064603 (2002).

[3] K. Wisshak, F. Voss, C. Arlandini, F. Bečvář, O. Straniero, R. Gallino, M. Heil, F. Käppeler, M. Krtička, S. Masera, R. Reifarth, and C. Travaglio, Phys. Rev. Lett. **87**, 251102 (2001).

[4] H. Beer, F. Käppeler, K. Yokoi, and K. Takahashi, Ap. J. **287**, 388 (1984).

[5] R.R. Winters, F. Käppeler, K. Wisshak, A. Mengoni, and G. Reffo, Ap. J. **300**, 41 (1986).

[6] K. Wisshak, K. Guber, F. Voss, F. Käppeler, and G. Reffo, Phys. Rev. C **48**, 1401 (1993) and Report KfK-5067, Forschungszentrum Karlsruhe (1992).

[7] K. Wisshak, F. Voss, F. Käppeler, K. Guber, L. Kazakov, N. Kornilov, M. Uhl, and G. Reffo, Phys. Rev. C. **52**, 2762 (1995).

[8] K.A. Toukan, K. Debus, F. Käppeler, and G. Reffo, Phys. Rev. C **51**, 1540 (1995).

[9] J. Best, H. Stoll, C. Arlandini, S. Jaag, F. Käppeler, K. Wisshak, A. Mengoni, G. Reffo, and T Rauscher, Phys. Rev. C **64**, 015801 (2001).

[10] R. Reifarth, C. Arlandini, M. Heil, F. Käppeler, P.V. Sedychev, A. Mengoni, M. Herman, T. Rauscher, R. Gallino, and C. Travaglio, Ap. J. **582**, 064603 (2003).

[11] S. Jaag and F. Käppeler, Phys. Rev. C **51**, 3465 (1995)

[12] U. Abbondanno, *et al.* Nucl. Instr. Meth. A **521**, 454 (2004).

[13] M. Heil and the n_TOF collaboration, Proc. of the XI Int. Seminar on Interactions of Neutrons with Nuclei, JINR Dubna, Dubna, Russia, May 28-31, 2003 (in press).

[14] K. Wisshak, F. Voss, F. Käppeler, and G. Reffo, Phys. Rev. C **45**, 2470 (1992).

[15] K. Wisshak, K. Guber, F. Käppeler, J. Krisch, H. Müller, G. Rupp, and F. Voss, Nucl. Instr. Meth. A **292**, 595 (1990).

[16] G.J. Kirouac and H.M. Eiland, Phys. Rev. C **11**, 895 (1975).

[17] F. H. Fröhner, Technical report, GA-8380, Gulf General Atomic (1968).

[18] C. Nordborg, H. Gruppelaar, and M. Salvatores, in *Nuclear Data for Science and Technology*, edited by S. Qaim (Springer, Berlin, 1992), p. 782.

[19] V. McLane, C.L. Dunford, and P.F. Rose, in *Neutron Cross Sections, Vol. 2,* (Academic Press, New York, 1988).

[20] K. Wisshak, F. Voss, F. Käppeler, L. Kazakov, and G. Reffo, Report FZKA 5967, Forschungszentrum Karlsruhe (1997).

[21] K. Wisshak, F. Voss, F. Käppeler, and G. Reffo, Phys. Rev. C. **42**, 1731 (1990).

[22] F. Voss, K. Wisshak, C. Arlandini, F. Käppeler, L. Kazakov, and T. Rauscher, Phys. Rev. C **59**, 1154 (1999).

[23] A. Gilbert and A.G.W. Cameron, Can. J. Phys. **43**, 1446 (1965).

[24] J. F. Mughabghab, M. Divadeenam, and N. E. Holden, in *Neutron Cross Sections, Vol. 1, Part A* (Academic Press, New York, 1981).

[25] J. Apostolakis, Technical Report, CERN, GEANT library (available from: www.cern.ch).

[26] M. Heil, R. Reifarth, M.M. Fowler, R.C. Haight, F. Käppeler, R.S. Rundberg, E.H. Seabury, J.L. Ullmann, J.B. Wilhelmy, and K. Wisshak, Nucl. Instr. Meth. **A 459**, 229 (2001).

[27] F. Bečvář, in *Capture Gamma-Ray Spectroscopy and Related Topics*, edited by S. Wender, AIP Conference Proceedings 529 (AIP, New York, 2000), p. 504.

[28] F. Bečvář, Nucl. Instr. Meth. A **417**, 434 (1998).

[29] K. Wisshak, F. Voss, F. Käppeler, L. Kazakov, and M. Krtička, Report FZKA 6962, Forschungszentrum Karlsruhe (2004).

[30] A. Artna-Cohen, Nucl. Data Sheets **79**, 1 (1996).

[31] F. Voss, K. Wisshak, K. Guber, F.Käppeler, and G. Reffo, Phys. Rev. C **50**, 2582 (1994).

[32] R. L. Macklin, private communication (unpublished).

[33] W. Ratynski and F. Käppeler, Phys. Rev. C **37**, 595 (1988).

[34] J. Kopecky, J.-Ch. Sublet, J.A. Simpson, R.A. Forrest, and D. Nierop, Report INDC(NDS)-362, (International Atomic Energy Agency, Vienna, 1997).

[35] V.N. Kononov, B.D. Yurlov, E.D. Poletaev, and V.M. Timokhov, Sov. J. Nucl. Phys. **26**, 500 (1977).

[36] J.H. Gibbons, R.L. Macklin, P.D. Miller, and J.H. Neiler, Phys. Rev. **122**, 182 (1961).

[37] S.A. Reynolds, J.F. Emery, and E.I. Wyatt, Nucl. Sci. Eng. **22**, 46 (1968).

[38] B. Singh, Nuclear Data Sheets **80**, 263 (1997).

[39] K.F. Flynn, L.E. Glendenin, and E.P. Steinberg, Nucl. Sci. Eng. **22**, 416 (1965).

[40] T. Rauscher and F.-K. Thielemann, Atomic Data Nucl. Data Tables **75**, 1 (2000).

[41] M. Harris, Astrophys. Space Sci. **77**, 357 (1981).

[42] J. Holmes, S. Woosley, W. Fowler, and B. Zimmernan, Atomic Data Nucl. Data Tables **18**, 305 (1976).

[43] H. Beer, F. Voss, and R.R. Winters, Astrophys. J. Suppl. **80**, 403 (1992).

[44] U. Abbondanno, *et al.* Phys. Rev. Lett. (submitted).